

A MATHEMATICAL MODEL FOR THE SULPHUR DIOXIDE AGGRESSION TO CALCIUM CARBONATE STONES: NUMERICAL APPROXIMATION AND ASYMPTOTIC ANALYSIS*

D. AREGBA-DRIOLLET[†], F. DIELE[‡], AND R. NATALINI[§]

Abstract. We introduce a degenerate nonlinear parabolic system that describes the chemical aggression of calcium carbonate stones under the attack of sulphur dioxide. For this system, we present some finite element and finite difference schemes to approximate its solutions. Numerical stability is given under suitable CFL conditions. Finally, by means of a formal scaling, the qualitative behavior of the solutions for large times is investigated, and a numerical verification of this asymptotics is given. Our results are in qualitative agreement with the experimental behavior observed in the chemical literature.

Key words. chemical aggression, porous media, nonlinear parabolic equations, fast reaction limit, free boundary problems, finite element, finite differences

AMS subject classifications. Primary, 65M06; Secondary, 76M20, 76R, 82C40

DOI. 10.1137/S003613990342829X

1. Introduction. In this paper we introduce and investigate a differential model to describe the evolution of the chemical action of SO_2 (sulphur dioxide) in CaCO_3 (calcium carbonate) stones. Let Ω be a given region in \mathbb{R}^n , with $n = 1, 2, 3$, namely, our stone specimen. Our basic equations read, in their adimensional form, as

$$(1.1) \quad \begin{cases} \partial_t(\varphi(c)s) - \nabla \cdot (\varphi(c)\nabla s) = -\varphi(c)sc, \\ \partial_t c = -\varphi(c)sc, \end{cases}$$

for $x \in \Omega$ and $t \in \mathbb{R}$. Here c and s are both nonnegative, since c stands for the local density of CaCO_3 and s for the porous concentration of SO_2 , namely, the concentration taken with respect to the volume of the pores; here the porosity φ is a linear function of the density c . For this problem we also have to specify the initial and boundary conditions, according to the problem under examination.

There is an extensive chemical literature about the deterioration mechanisms of natural building stones [22, 23, 14, 26, 18, 8] in connection with problems concerning both modern and historical buildings. Acidity in the air is essentially caused by pollutants, such as sulphur and nitrogen oxides, which are emitted into the atmosphere by sources related to industry, transportation, and heating. These species are transformed, through complex reaction pathways, into gaseous nitric and nitrous acids and into acidic sulphates as suspended particles. Although in recent years the levels of

*Received by the editors May 20, 2003; accepted for publication (in revised form) December 19, 2003; published electronically June 22, 2004. The research activity reported in this paper was partially conducted within the European Union RTN project FRONTS-SINGULARITIES: HPRN-CT-2002-00274 and the European Union RTN HYKE project HPRN-CT-2002-00282.

<http://www.siam.org/journals/siap/64-5/42829.html>

[†]Mathématiques Appliquées de Bordeaux, Université Bordeaux 1, 351 cours de la Libération, F-33405 Talence, France (aregba@math.u-bordeaux.fr).

[‡]Istituto per le Applicazioni del Calcolo “M. Picone,” Consiglio Nazionale delle Ricerche, Sez. Bari, Via Amendola 122/I, I-70126 Bari, Italy (f.diele@iac.cnr.it).

[§]Istituto per le Applicazioni del Calcolo “M. Picone,” Consiglio Nazionale delle Ricerche, Viale del Policlinico 137, I-00161 Rome, Italy (r.natalini@iac.cnr.it).

pollution in the urban areas of Europe have decreased, levels of HNO₃ and other aggressive pollutants such as sulphur dioxide and ozone have remained consistent. As is well known, SO₂ and NO₃ react with calcium carbonate stones to form sulphates and nitrates, which, due to their solubility in water, may be drained away or, if protected from the rain, may form crusts, which eventually exfoliate; see [8, 5]. Observe that the chemical deterioration is mainly expected to occur when the surface is wet. There is in fact a strong experimental relationship between deterioration and time of wetness [14].

Effective simulation tools seem to be crucial in considering the fine-scale evolution of reaction pathways, possibly in complex geometries, as requested by an improved policy of prevention and monitoring of chemical damage on historical monuments. For instance, it should be important to assist stakeholders to assign a degree of priority for an optimal scheduling of cleaning operations, also taking into account the local geometry and the exposure of the concerned stones. Actually, the standard methods used for studying the evolution of this kind of damage have been the development of models of atmospheric corrosion; they are based on the statistic determination on the ratio of dose and response of the materials. For instance, the Lipfert formula [19] was applied, using an extended database containing values taken in the field (i.e., meteorological value and pollution of the air). If this procedure could be meaningful for the determination of corrosion for civil uses, this approach is clearly insufficient for artistic and historical artwork.

In this paper we introduce a different approach in the framework of hydrodynamic models by using some basic physical relations, the balance laws of the chemical reactions, and the Fick law, and by neglecting the permeability of the medium. As a particular feature, the model takes into account the effects of sulphation on carbonate rocks, by assuming a direct (linear) dependence of porosity and diffusivity on the density of calcium carbonate. The main issue of our model will be a proper determination of the thickness of the gypsum crust (CaSO₄ · 2H₂O) formed as a product of the reaction of SO₂ with calcium carbonate stones. There are two main advantages in this approach: it is possible to solve numerically the equations by finite element or finite difference methods, and also in several space dimensions and for geometrically complex domains; time asymptotic analysis in one space dimension yields a precise characterization of the behavior of the limit solutions, which are expressed in terms of a simple free boundary problem.

Global existence of smooth solutions for this system is considered in a separate work [12]. A more general model, which includes convective effects due to the pressure gradient, for stones with a greater permeability, will be introduced and studied in [1].

The paper is organized as follows. In section 2, we introduce in some detail a basic model starting from the main ideas of macroscopic modeling of filtration in porous media [3, 21]. Next, we propose some different numerical approximations, to both finite element and finite difference schemes, for the one-dimensional case, by proving some rigorous nonlinear stability and positivity results, under some proper CFL conditions. Numerical tests are given for comparison of the accuracy of different schemes. Finally, we investigate the asymptotic behavior of solutions and assess the agreement of the model with experimental tests. By scaling arguments, it is possible to show that the limit profile of solutions, for the case of the half-line $x > 0$ and with Dirichlet boundary conditions for s at $x = 0$, is given by the solution of a simple one-phase Stefan problem [20]. This approach is inspired by a related paper [15], where a similar model was considered, but with constant porosity and diffusivity.

The analytical verification of this asymptotic behavior will be considered in a future work. Here we just give a numerical verification, which actually yields quite precise information on the propagation of the main front and on the rate of convergence of the solution toward its limit profile.

In particular, it is worth mentioning that the limit profile has a free boundary $\zeta(t)$ which gives the right limit of the gypsum crust and evolves according to a diffusive law:

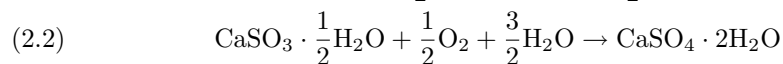
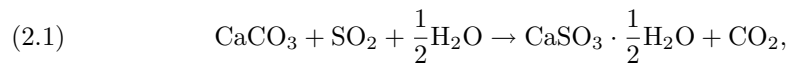
$$(1.2) \quad \zeta(t) = C\sqrt{t}.$$

This behavior is in good qualitative agreement with experimental data (see [22, 23, 18]) and in particular with the results of the new laboratory tests performed in [10], and the possibility of a successful calibration of the model against laboratory and in situ tests is shown.

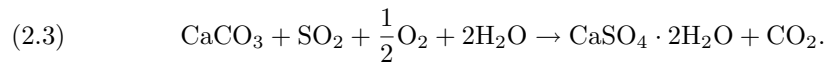
2. Derivation of the model. In [18, 8] the authors conducted experimental studies involving the exposure of different types of marble to 10 and 300 ppm SO₂ atmospheres. It was then possible to estimate practically the extent of damage to marble due to an industrial environment. Analogous experiments were conducted with dolomite rocks [26]. Other laboratory tests and in situ measurements can be found in [22, 23, 6, 5].

Considering the mathematical description of the time evolution of the sulphation process, some models were proposed in [18] to give some measurements of the main physicochemical parameters. The different regions and time regimes were described by different parameters and then matched to fit the experimental behavior of the reaction. Here we develop a single mathematical model that in principle can take into account the full behavior of the solutions.

The path of reaction of SO₂ with calcite is revealed by the X-ray diffraction counts, which suggest that the reaction occurs in the following manner [2, 18]:



(see also [6, 9, 7, 26, 25]). The CaSO₃ (calcium sulphite) reaches equilibrium soon after the initial reaction, and then the amount of gypsum continues to increase with the progress of the reaction. Therefore we can assume a simplified one-step reaction:



We neglect all heat effects and assume the air contains enough water to give rise to the reaction. Moreover, we assume that the change in concentrations of oxygen (O₂), water (H₂O), and carbon dioxide (CO₂) does not affect the reaction.

Let Ω be the domain occupied by the specimen of calcite under consideration and set ρ_s for the concentration of SO₂; c for the density of CaCO₃; and g for the density of CaSO₄ · 2H₂O. All quantities are defined with respect to the whole volume, incorporating both solid and gaseous material, and depend on the position $x \in \Omega$ and on time t . Since we are including the bulk volume in the definition of c , g , ρ_s , we will call them total concentrations or densities. We will define later the porous concentrations for SO₂.

Following [3], we assume that the total concentrations ρ_s and c satisfy the balance laws,

$$(2.4) \quad \partial_t \rho_s + \nabla \cdot (\rho_s \mathbf{V}_s) = \dot{r}_s,$$

$$(2.5) \quad \partial_t c = \dot{r}_c,$$

where \mathbf{V}_s is the sulphur dioxide “fluid” velocity and \dot{r}_s, \dot{r}_c are rates of production (or consumption) of sulphur dioxide and calcite.

Following the usual model for the rate of production, we have

$$(2.6) \quad \dot{r}_s = -m_s \omega, \quad \dot{r}_c = -m_c \omega.$$

Here, m_s, m_c are the masses of single molecules of sulphur dioxide and calcite, and, to complete the notations, let us set m_g for the molecular mass of gypsum. The quantity $\omega > 0$ measures the rate of reaction and according to [18] is given by

$$(2.7) \quad \omega = A \left(\frac{\rho_s}{m_s} \right) \left(\frac{c}{m_c} \right).$$

In general, the constant A depends on the temperature and on the activation energy. In the present paper we shall neglect this dependence.

Assuming initial densities c_0 and g_0 , for calcite and gypsum, we have the relation

$$(2.8) \quad c + \frac{m_c}{m_g} g = c_0 + \frac{m_c}{m_g} g_0,$$

which expresses the density of gypsum as a function of calcite.

Next, we introduce the porosity of the calcite specimen φ , which cannot be assumed constant, since the transformation of calcite in gypsum alters the volume of void (occupied by air and sulphur dioxide). Therefore, following [24], it is reasonable to regard it as a function of the amount of gypsum or, equivalently, as a function of the amount of calcite, that is, $\varphi = \varphi(c)$.

Let φ_0 be the porosity of the pure calcite specimen, i.e., for $c = c_0, g = 0$, and $\varphi_{\tilde{g}}$ the porosity of the final sulphate product, when all the calcium carbonate has been converted in gypsum, namely, when $c = 0, \tilde{g} = \frac{m_a}{m_c} c_0$. Then, according to the rigorous derivation in [1], we can express the porosity of the specimen during the reaction as a linear combination of these porosities:

$$(2.9) \quad \varphi(c) = \varphi_{\tilde{g}} + (\varphi_0 - \varphi_{\tilde{g}}) \frac{c}{c_0}.$$

We denote by s the porous concentration of SO₂, which is defined as the concentration taken with respect to the volume of the pores, which is related to the total concentration by

$$(2.10) \quad \rho_s = \varphi(c) s.$$

The seepage velocity \mathbf{v}_s is related to the fluid velocity \mathbf{V}_s by the classical Dupuit–Forchheimer relation

$$(2.11) \quad \mathbf{v}_s = \varphi(c) \mathbf{V}_s.$$

The balance laws for ρ_s and c become

$$(2.12) \quad \partial_t(\varphi(c)s) + \nabla \cdot (s\mathbf{v}_s) = - \left(\frac{A}{m_c} \right) \varphi(c)sc,$$

$$(2.13) \quad \partial_t c = - \left(\frac{A}{m_s} \right) \varphi(c)sc.$$

To close the system (2.12)–(2.13), we need an expression for the seepage velocity \mathbf{v}_s . In the following we make the main assumption of our model, namely, that all the contributions given by the pressure gradient to the seepage velocity can be neglected. As shown in [1], this corresponds to a zero permeability limit, which is a realistic assumption for many species of marble.

Therefore, we shall express \mathbf{v}_s by the classical Fick law [21],

$$(2.14) \quad s\mathbf{v}_s = -D(c)\nabla s,$$

where $D(c) = d\varphi(c)$, and d is the (scalar) effective molecular diffusive coefficient. This yields

$$(2.15) \quad \partial_t(\varphi(c)s) = - \left(\frac{A}{m_c} \right) \varphi(c)sc + d\nabla \cdot (\varphi(c)\nabla s),$$

$$(2.16) \quad \partial_t c = - \left(\frac{A}{m_s} \right) \varphi(c)sc.$$

System (2.15)–(2.16) forms a closed set of nonlinear degenerate parabolic differential equations which have to be supplemented by initial conditions at time $t = 0$ for s and c , and by Dirichlet or Neumann boundary conditions for s . Let us also notice that in general we do not expect to give any boundary condition for c . Clearly, it is also possible to consider system (2.15)–(2.16) as a one parabolic equation coupled with an ordinary differential equation. Unfortunately, it is difficult to use this remark, since we have to take into account the strong coupling between s and c into the divergence term.

It is easy to see that we can recover the scaled model (1.1) just by taking the new variables

$$(2.17) \quad y = \sqrt{\frac{A}{dm_c}}x, \quad \tau = \frac{A}{m_c}t, \quad \tilde{s} = \frac{m_c}{m_s}s.$$

To improve the physical accuracy of our model, it should be possible to consider three main modifications. The first is to assume the dependence of the reaction rate A on the internal temperature and degree of wetness by introducing two supplementary equations related to the evolution of these quantities for some given initial and boundary conditions.

Another important modification arises if, according to [13], we consider a more general nonlinear Fick law,

$$(2.18) \quad s\mathbf{v}_s(Bs|\mathbf{v}_s| + 1) = -D\nabla s,$$

where B is the high concentration coefficient. The form (2.18) of the Fick law is best suited when the gradient of the concentration is very high.

Finally, let us mention that a more accurate model, which takes into account both the pressure gradient effects due to the Darcy law and the diffusivity given by the Fick law, will be considered in [1].

3. Numerical approximation in one space dimension. In this section we construct numerical schemes for the one-dimensional version of model (1.1),

$$(3.1) \quad \begin{cases} \partial_t \rho_s - \partial_x(\varphi(c)\partial_x s) = -\rho_s c, \\ \partial_t c = -\rho_s c \end{cases}$$

for $x \in [0, 1]$, $t \geq 0$ and where we recall that $\rho_s = \varphi(c)s$ and $\varphi(c)$ is given by (2.9). In the following, we shall assume that the initial calcite density c_0 is a positive constant. Then, setting $\alpha = \frac{1}{c_0}(\varphi_0 - \varphi_{\bar{g}})$ and $\beta = \varphi_{\bar{g}}$, we can rewrite the function $\varphi(c)$ in the following form:

$$(3.2) \quad \varphi(c) = \alpha c + \beta.$$

In what follows, we shall assume that

$$(3.3) \quad \varphi_0 > \varphi_{\bar{g}},$$

with $\alpha, \beta > 0$ and $0 < \beta \leq \varphi(c) \leq \alpha c_0 + \beta < 1$. The case $\varphi_0 < \varphi_{\bar{g}}$ is similar and can be considered by using the same arguments.

As initial conditions we have

$$(3.4) \quad \begin{cases} \rho_s(x, 0) = 0, \\ c(x, 0) = c_0, \end{cases}$$

where c_0 is a positive constant, and we impose the boundary conditions,

$$(3.5) \quad \begin{cases} \rho_s(0, t) = \rho_{s0}, \\ \frac{\partial \rho_s}{\partial x}(1, t) = 0. \end{cases}$$

Here ρ_{s0} is a positive constant. The case where ρ_{s0} is a bounded measurable positive function can be treated in the same way.

It is easy to see that s satisfies the same initial condition as ρ_s , and the boundary conditions read as

$$(3.6) \quad \begin{cases} s(0, t) = \frac{\rho_{s0}}{\varphi(c(0, t))}, \\ \frac{\partial s}{\partial x}(1, t) = 0 \end{cases}$$

with

$$(3.7) \quad c(0, t) = c_0 e^{-\rho_{s0} t}.$$

Two methods of solving this problem are under consideration. First, we use a finite element method, looking for s as a continuous piecewise linear function and c as a piecewise constant function. The second method is a finite difference scheme, where the main unknowns are ρ_s and c . For some problems in one space dimension, finite element methods have an interpretation in terms of finite differences via mass lumping and staggered variables. However, the philosophies are quite different, and our aim is to study afterward two- or three-dimensional systems, with possibly complicated geometries. On the other hand, for the methods presented in this paper it is easier to modify the time discretization for the finite difference schemes. We compare these approaches and analyze the effect of time discretization modifications.

3.1. A finite element method. Following [12], we look for a smooth solution (s, c) of (3.1), (3.4), (3.6).

3.1.1. The scheme. To deal with the nonhomogeneous Dirichlet condition, we introduce the unknown $\sigma(x, t) = s(x, t) - s(0, t)$, and we denote $H = \{u \in H^1(]0, 1[), u(0) = 0\}$. The first equation of (3.1) can be written as

$$\partial_t(\varphi\sigma) - \partial_x(\varphi(c)\partial_x\sigma) = F(\sigma, c, t),$$

and a variational formulation of the problem is as follows: find $(\sigma, c) \in C^1([0, +\infty[, H \times L^2(]0, 1[))$ such that for all $(p, q) \in H \times L^2(]0, 1[)$,

$$(3.8) \quad \begin{cases} \partial_t \int_{]0,1[} \varphi\sigma p dx + \int_{]0,1[} \varphi\partial_x\sigma\partial_x p dx = \int_{]0,1[} pF dx, \\ \partial_t \int_{]0,1[} cq dx = - \int_{]0,1[} \varphi(\sigma + s(0, \cdot))cq dx. \end{cases}$$

Let us define a regular mesh

$$[0, 1] = \cup_{1 \leq i \leq N} [x_i, x_{i+1}], \quad x_i = (i - 1)\Delta x, \quad \Delta x = 1/N.$$

We denote by $\{p_i, i = 1, \dots, N + 1\}$ the classical P1 basis functions:

$$p_i(x) = \begin{cases} \frac{x-x_{i-1}}{\Delta x} & \text{if } x \in [x_{i-1}, x_i], \\ \frac{x_{i+1}-x}{\Delta x} & \text{if } x \in [x_i, x_{i+1}], \\ 0 & \text{else.} \end{cases}$$

For $i = 1, \dots, N$, we denote by q_i the characteristic function of $[x_i, x_{i+1}[$.

The solution (s, c) is approximated by

$$s_h(x, t) = \sum_{i=1}^{N+1} \xi_i(t)p_i(x), \quad c_h(x, t) = \sum_{k=1}^N \eta_k(t)q_k(x).$$

Moreover, we define $\rho_{s,h}(x, t) = \varphi(c_h(x, t))s_h(x, t)$.

The unknowns for s_h are located on the nodes, while the ones for c_h can be considered as approximations of the mean value of c on each cell $[x_i, x_{i+1}]$. The Dirichlet boundary condition at $x = 0$ is taken into account by putting $\xi_1(t) = \rho_{s0}/\varphi(\eta_1(t))$, according to (3.6), so that $\sigma_h = s_h - \xi_1 p_1$ and $(\sigma_h, c_h) \in C^1([0, +\infty[, V \times W)$, where $V = \text{lin}\{p_i, i = 2, \dots, N + 1\}$ and $W = \text{lin}\{q_i, i = 1, \dots, N\}$.

In practice, as usual for this kind of problem we write a (false) variational approach formulation with $N + 1$ basis functions $\{p_1, \dots, p_{N+1}\}$, and we put the Dirichlet condition a posteriori: for all $i = 1, \dots, N + 1$, for all $k = 1, \dots, N$,

$$(3.9) \quad \begin{cases} \partial_t \int_{]0,1[} \varphi_h s_h p_i dx + \int_{]0,1[} \varphi_h \partial_x s_h \partial_x p_i dx = - \int_{]0,1[} \varphi_h s_h c_h p_i dx, \\ \partial_t \int_{]0,1[} c_h q_k dx = - \int_{]0,1[} \varphi_h s_h c_h q_k dx. \end{cases}$$

In this formula, φ_h is defined by

$$\varphi_h = \varphi(c_h).$$

The first set of equations in (3.9) is a differential system which is linear with respect to ξ :

$$\begin{aligned} & \partial_t \sum_{j=1}^{N+1} \xi_j \int_{]0,1[} \varphi_h p_j p_i dx + \sum_{j=1}^{N+1} \xi_j \int_{]0,1[} \varphi_h \partial_x p_j \partial_x p_i dx \\ &= - \sum_{j=1}^{N+1} \xi_j \int_{]0,1[} \varphi_h c_h p_j p_i dx, \quad i = 1, \dots, N + 1. \end{aligned}$$

As $\varphi_h = \sum_{k=1}^N \varphi(\eta_k) q_k$, it can be summarized as

$$(3.10) \quad \partial_t(M(\eta)\xi) + K(\eta)\xi = 0.$$

Denoting $\varphi(\eta_k) = \varphi_k$, the matrix $M(\eta)$ is defined by

$$M(\eta) = \frac{\Delta x}{6} \begin{pmatrix} 2\varphi_1 & \varphi_1 & 0 & \dots & 0 \\ \varphi_1 & 2(\varphi_1 + \varphi_2) & \varphi_2 & \dots & 0 \\ \dots & \dots & \dots & \dots & \dots \\ 0 & \dots & \varphi_{N-1} & 2(\varphi_{N-1} + \varphi_N) & \varphi_N \\ 0 & \dots & 0 & \varphi_N & 2\varphi_N \end{pmatrix},$$

and the matrix $K(\eta)$ is defined by

$$\begin{aligned} K(\eta) &= \frac{1}{\Delta x} \begin{pmatrix} \varphi_1 & -\varphi_1 & 0 & \dots & 0 \\ -\varphi_1 & \varphi_1 + \varphi_2 & -\varphi_2 & \dots & 0 \\ \dots & \dots & \dots & \dots & \dots \\ 0 & \dots & -\varphi_{N-1} & \varphi_{N-1} + \varphi_N & -\varphi_N \\ 0 & \dots & 0 & -\varphi_N & \varphi_N \end{pmatrix} \\ &+ \frac{\Delta x}{6} \begin{pmatrix} 2\varphi_1\eta_1 & \varphi_1\eta_1 & 0 & \dots & 0 \\ \varphi_1\eta_1 & 2(\varphi_1\eta_1 + \varphi_2\eta_2) & \varphi_2\eta_2 & \dots & 0 \\ \dots & \dots & \dots & \dots & \dots \\ 0 & \dots & \varphi_{N-1}\eta_{N-1} & 2(\varphi_{N-1}\eta_{N-1} + \varphi_N\eta_N) & \varphi_N\eta_N \\ 0 & \dots & 0 & \varphi_N\eta_N & 2\varphi_N\eta_N \end{pmatrix}. \end{aligned}$$

The second equation of problem (3.9) can be written as

$$\Delta x \partial_t \eta_k = -\eta_k(\alpha\eta_k + \beta) \sum_{j=1}^{N+1} \xi_j(t) \int_{]x_k, x_{k+1}[} p_j(x) dx, \quad k = 1, \dots, N$$

or, equivalently,

$$(3.11) \quad \partial_t \eta_k = -\frac{(\xi_k + \xi_{k+1})}{2} \eta_k(\alpha\eta_k + \beta) = -\gamma_k \eta_k(\alpha\eta_k + \beta), \quad k = 1, \dots, N.$$

We now discretize in time. The approximated quantities at time $t_n = n\Delta t$ are denoted with a superscript n , and for $t \in [t_n, t_{n+1}[$ we put $s_h(x, t) = s_h^n(x)$, $c_h(x, t) = c_h^n(x)$.

In view of initial and boundary data we take

$$\begin{cases} \xi_1^0 = \frac{\rho_{s0}}{\varphi(c_0)}, \quad \xi_j^0 = 0 & \text{for } j = 2, \dots, N + 1, \\ \eta_k^0 = c_0 & \text{for } k = 1, \dots, N. \end{cases}$$

We first discretize (3.11) by fixing $\xi = \xi^n$ and solving exactly the equation. As α and β are positive, if the ξ_j^n and η_k^n are nonnegative, without any time step restriction, we obtain the intermediate value $\eta_k^{n+1/2}$:

$$(3.12) \quad \eta_k^{n+1/2} = \beta \eta_k^n \frac{e^{-\gamma_k \beta \Delta t}}{\alpha \eta_k^n + \beta - \alpha \eta_k^n e^{-\gamma_k \beta \Delta t}}.$$

Then, we solve the differential system (3.10) by the θ method ($\theta \in [0, 1]$):

$$(3.13) \quad \frac{M(\eta^{n+1/2})\xi^{n+1} - M(\eta^n)\xi^n}{\Delta t} + (1 - \theta)K(\eta^n)\xi^n + \theta K(\eta^{n+1/2})\xi^{n+1} = 0.$$

This is a linear tridiagonal system $UX = G$.

The boundary condition is taken into account by replacing g_1 by $\rho_{s0}/\varphi(\eta_1^{n+1/2})$, g_2 by $g_2 - u_{21}\rho_{s0}/\varphi(\eta_1^{n+1/2})$, u_{1j} by δ_{1j} , and u_{i1} by δ_{i1} . This modified linear system is symmetric and positive and can be easily solved, for example, by a Choleski method.

This method is first order in time, even if $\theta = 1/2$, because the matrices M and K depend on $\eta(t)$. When ξ^{n+1} is computed we can set

$$\eta_k^{n+1} = \eta_k^{n+1/2}$$

or improve the approximation with the second order Heun method: we solve exactly (3.11) with $\xi = \xi^{n+1}$ and initial value $\eta_k^{n+1/2}$. We obtain a second intermediate value $\eta_k^{n+1/2,1}$, and, finally, we set

$$(3.14) \quad \eta_k^{n+1} = \frac{\eta_k^n + \eta_k^{n+1/2,1}}{2}.$$

In the following, we call this finite element method FE- θ .

3.1.2. Stability. It is well known that the discrete maximum principle does not always hold in the finite element method. We have the following stability results.

PROPOSITION 3.1. *Suppose that $\theta \in]1/3, 1]$ and $\Delta x^2 < \frac{3(3\theta-1)}{c_0}$. If the time step satisfies the condition*

$$(3.15) \quad \frac{\Delta x^2}{\theta(6 - c_0 \Delta x^2)} < \Delta t \leq \frac{\Delta x^2}{(1 - \theta)(3 + c_0 \Delta x^2)},$$

then for all $x \in [0, 1]$, $c_h(x, \cdot)$ is a nonincreasing function of t and for all $t \geq 0$,

$$\rho_{s,h}(x, t) \geq 0, \quad c_h(x, t) \in]0, c_0].$$

Moreover, the condition (3.15) is not empty.

Proof. The result is true for $t \in [0, t_1[$. Suppose that for all $j = 1, \dots, N + 1$ and all $k = 1, \dots, N$ we have $\xi_j^n \geq 0$ and $\eta_k^n \in]0, c_0]$. In view of (3.11) and (3.12), $0 < \eta_k^{n+1/2} \leq \eta_k^n$, and thus $0 < \varphi_k^{n+1/2} \leq \varphi_k^n$.

After the modifications due to boundary conditions, the system (3.13) has an $N \times N$ symmetric irreducibly diagonally dominant matrix, still denoted $U = M^{n+1/2} + \Delta t \theta K^{n+1/2}$. Hence, U^{-1} is positive if $u_{ij} < 0$ for $j = i \pm 1$ and $u_{ii} > 0$ for all i [27].

In the right-hand side, we have for $i \geq 2$,

$$g_i = \sum_{j=i-1}^{i+1} (m_{ij}^n - (1 - \theta)\Delta t k_{ij}^n) \xi_j^n, \quad \xi_1^n = \rho_{s0}/\varphi_1^n,$$

and

$$\begin{aligned} g_{2,\text{modified}} &= g_2 - \frac{u_{21}\rho_{s0}}{\varphi_1^{n+1/2}} \\ &= \sum_{j=2}^3 (m_{2j}^n - (1 - \theta)\Delta t k_{2j}^n) \xi_j^n \\ (3.16) \quad &+ \frac{\Delta t}{\Delta x} \left[1 - \frac{\Delta x^2}{6} \eta_1^n + \theta \frac{\Delta x^2}{6} (\eta_1^n - \eta_1^{n+1/2}) \right] \rho_{s0}. \end{aligned}$$

Due to the condition on Δx and the fact that η is nonincreasing, the third line is nonnegative. Consequently, the positivity is preserved if the following requirements are fulfilled:

$$\begin{aligned} (3.17) \quad &m_{ij}^{n+1/2} + \theta \Delta t k_{ij}^{n+1/2} < 0 \quad \text{for } j = i \pm 1, \quad i \geq 2, \\ &m_{ii}^{n+1/2} + \theta \Delta t k_{ii}^{n+1/2} > 0 \quad \text{for all } i \geq 2, \\ &m_{ij}^n - (1 - \theta)\Delta t k_{ij}^n \geq 0 \quad \text{for all } i \geq 2, \quad j. \end{aligned}$$

For $j \neq i$, we have to consider $j = i - 1$:

$$k_{ij} = -\frac{\varphi_{i-1}}{\Delta x} + \frac{\Delta x}{6} \varphi_{i-1} \eta_{i-1} \leq 0.$$

Moreover, k_{ii} is positive. Hence, the second requirement of (3.17) is fulfilled. So is the third for $i \neq j$.

Consequently, we have to satisfy for all i and $j = i \pm 1$,

$$(3.18) \quad -\frac{m_{ij}^{n+1/2}}{\theta k_{ij}^{n+1/2}} < \Delta t \leq \frac{m_{ii}^n}{(1 - \theta)k_{ii}^n}.$$

We have for $2 \leq i \leq N$,

$$\begin{aligned} (3.19) \quad \frac{m_{ii}}{(1 - \theta)k_{ii}} &= \frac{\Delta x(\varphi_{i-1} + \varphi_i)}{3(1 - \theta) \left(\frac{\varphi_{i-1} + \varphi_i}{\Delta x} + \frac{\Delta x(\varphi_{i-1}\eta_{i-1} + \varphi_i\eta_i)}{3} \right)} \\ &\geq \frac{\Delta x^2}{(1 - \theta)(3 + c_0\Delta x^2)}. \end{aligned}$$

For $i = N + 1$ the same lower estimate holds. For $j = i - 1$,

$$\begin{aligned} (3.20) \quad -\frac{m_{ij}}{\theta k_{ij}} &= \frac{\Delta x \varphi_{i-1}}{6\theta \left(\frac{\varphi_{i-1}}{\Delta x} - \frac{\Delta x \varphi_{i-1} \eta_{i-1}}{6} \right)} \\ &\leq \frac{\Delta x^2}{\theta(6 - c_0\Delta x^2)}. \end{aligned}$$

The fact that condition (3.15) is not empty, i.e.,

$$\frac{\Delta x^2}{\theta(6 - c_0\Delta x^2)} < \frac{\Delta x^2}{(1 - \theta)(3 + c_0\Delta x^2)},$$

is ensured by the conditions $\Delta x^2 < \frac{3(3\theta-1)}{c_0}$ and $\theta > 1/3$.

As it is enough to consider the case $\eta^{n+1} = \eta^{n+1/2}$, the proof is complete.

Remark 3.1. As usual, there is no upper limitation on Δt in the fully implicit case $\theta = 1$.

As far as we are concerned by the lower limitation on Δt , let us point out that, as is well known, if the matrix M is lumped, this limitation disappears.

If the data are small enough, we can prove a uniform bound for $\rho_{s,h}$. We fix the initial condition c_0 , and we determine for which values of ρ_{s0} the bound exists.

In what follows, we denote $\varphi_0 = \varphi(c_0)$.

PROPOSITION 3.2. *We make the same assumptions as in Proposition 3.1, and we take Δt satisfying condition (3.15). If, moreover, the two inequalities*

$$\begin{aligned} \text{(i)} \quad \Delta t &< \frac{\beta^2 - \alpha\varphi_0\rho_{s0}}{\beta^2\rho_{s0}}, \\ \text{(ii)} \quad \rho_{s0} &< \frac{\beta^2}{\alpha\varphi_0}, \end{aligned}$$

are true, then the numerical solution has the additional bound

$$(3.21) \quad 0 \leq \rho_{s,h}(x, t) \leq \frac{\varphi_0}{\beta} \rho_{s0}.$$

Let us point out that condition (i) on Δt does not restrict condition (3.15) if the space step Δx is small enough.

Proof. By Proposition 3.1 positivity is preserved, and for all $n \geq 0$ and $i \in \{1, \dots, N\}$ we have

$$(3.22) \quad 0 < \eta_i^{n+1/2} \leq \eta_i^n \leq c_0.$$

Let us denote $X_n = \max\{\xi_j^n, 1 \leq j \leq N + 1\}$. For all $(x, t) \in [x_i, x_{i+1}[\times [t_n, t_{n+1}[$

$$\rho_{s,h}(x, t) = \varphi(\eta_i^n) [\xi_i^n p_i(x) + \xi_{i+1}^n p_{i+1}(x)].$$

Therefore,

$$0 \leq \rho_{s,h}(x, t) \leq \varphi_0 X_n,$$

and we have to show that

$$(3.23) \quad X_n \leq \frac{\rho_{s0}}{\beta}.$$

This inequality is true for $n = 0$:

$$X_0 = \xi_1^0 = \frac{\rho_{s0}}{\varphi_0} \leq \frac{\rho_{s0}}{\beta}.$$

Consider $n \geq 0$ and suppose that X_n satisfies (3.23). If $X_{n+1} = \xi_1^{n+1}$, then

$$X_{n+1} = \frac{\rho_{s0}}{\varphi_1^{n+1/2}} \leq \frac{\rho_{s0}}{\beta}.$$

Suppose now that $X_{n+1} = \xi_i^{n+1}$ with $2 \leq i \leq N$. Our goal is to show that $X_{n+1} \leq X_n$. By (3.17), we have

$$\sum_{j=i-1}^{i+1} \left(m_{ij}^{n+1/2} + \Delta t \theta k_{ij}^{n+1/2} \right) X_{n+1} \leq \sum_{j=i-1}^{i+1} \left(m_{ij}^n - \Delta t (1 - \theta) k_{ij}^n \right) X_n.$$

This inequality reads as

$$(3.24) \quad X_{n+1} \left[(\varphi_{i-1}^{n+1/2} + \varphi_i^{n+1/2}) + \Delta t \theta \left(\varphi_{i-1}^{n+1/2} \eta_{i-1}^{n+1/2} + \varphi_i^{n+1/2} \eta_i^{n+1/2} \right) \right] \\ \leq X_n \left[(\varphi_{i-1}^n + \varphi_i^n) - \Delta t (1 - \theta) \left(\varphi_{i-1}^n \eta_{i-1}^n + \varphi_i^n \eta_i^n \right) \right].$$

Using (3.22) and denoting

$$B = \frac{2}{\Delta x} \sum_{j=i-1}^{i+1} \left(m_{ij}^{n+1/2} + \Delta t \theta k_{ij}^{n+1/2} \right), \quad e_i = \eta_i^n - \eta_i^{n+1/2},$$

we obtain

$$B X_{n+1} \leq X_n \left[B + \alpha (e_{i-1} + e_i) - \Delta t \left(\varphi_{i-1}^{n+1/2} \eta_{i-1}^{n+1/2} + \varphi_i^{n+1/2} \eta_i^{n+1/2} \right) \right].$$

Hence, $X_{n+1} \leq X_n$ as soon as for all $i = 1, \dots, N$,

$$(3.25) \quad \alpha e_i - \Delta t \varphi_i^{n+1/2} \eta_i^{n+1/2} \leq 0.$$

By (3.12) we have

$$e_i = \eta_i^n \frac{\varphi_i^n (1 - e^{-\gamma_i \beta \Delta t})}{\alpha \eta_i^n + \beta - \alpha \eta_i^n e^{-\gamma_i \beta \Delta t}},$$

and (3.25) can be written as

$$\alpha \varphi_i^n (1 - e^{-\gamma_i \beta \Delta t}) - \Delta t \varphi_i^{n+1/2} \beta e^{-\gamma_i \beta \Delta t} \leq 0.$$

We are led to prove that $g(\Delta t) \leq 0$ with $g(\tau) = \alpha \varphi_0 (1 - e^{-\gamma_i \beta \tau}) - \tau \beta^2 e^{-\gamma_i \beta \tau}$.

We have $g(0) = 0$, and recalling that $\gamma_i = \frac{1}{2}(\xi_i^n + \xi_{i+1}^n)$, it is easy to see that $g'(\tau) < 0$ as soon as conditions (i) and (ii) are satisfied.

The case where $X_{n+1} = \xi_{N+1}^{n+1}$ is identical.

As it is enough to consider the case $\eta^{n+1} = \eta^{n+1/2}$, the proof is complete.

3.2. Finite difference schemes. Here the main variables are $u = (\rho_s, c)$. Denoting $S(u) = -\rho_s c$ we can write

$$(3.26) \quad \begin{cases} \partial_t \rho_s - \partial_x \left(\varphi(c) \partial_x \frac{\rho_s}{\varphi(c)} \right) = S(u), \\ \partial_t c = S(u). \end{cases}$$

3.2.1. The schemes. We again mesh $[0, 1]$ with a step $\Delta x = 1/N$, and we denote

$$\lambda = \frac{\Delta t}{\Delta x}, \mu = \frac{\Delta t}{\Delta x^2}, x_{m-1/2} = m\Delta x, x_m = (m - 0.5)\Delta x, X = (x_m)_{1 \leq m \leq N}.$$

We look for u_m^n , an approximation of $\frac{1}{\Delta x} \int_{x_{m-1/2}}^{x_{m+1/2}} u(x, t_n) dx$, and we set $\mathbf{u}(t) = (\mathbf{u}_1(t), \dots, \mathbf{u}_m(t))^T$, a smooth function such that $\mathbf{u}_m(t_n) = u_m^n$. We also denote by $u^n = (u_m^n)_{1 \leq m \leq N}$ the approximation of u at the time t_n .

It is clear that c_m^n plays the same role as η_k^n in the finite element method, while there is a staggering from vertices to cell centers between s and ρ_s .

The most simple, consistent approximation of $\partial_x(a(x)\partial_x r)$ by means of Taylor expansions is the following first order one:

$$(3.27) \quad \Delta_m(a, r) := \frac{(a_m + a_{m+1})(r_{m+1} - r_m) - (a_{m-1} + a_m)(r_m - r_{m-1})}{2\Delta x^2}.$$

Hence, a scheme which is comparable to the finite element method FE- θ is the following: $\rho_{s,m}^n$ being fixed, solve exactly the second equation of (3.26) and obtain

$$c_m^{n+1} = c_m^n e^{-\Delta t \rho_{s,m}^n}.$$

Then discretize the first equation of (3.26) as follows:

$$(3.28) \quad \frac{\rho_{s,m}^{n+1} - \rho_{s,m}^n}{\Delta t} - \Delta_m \left(\varphi^n, \frac{\rho_s^n}{\varphi^n} \right) = S((1 - \theta)\rho_{s,m}^n + \theta\rho_{s,m}^{n+1}, c_m^{n+1})$$

with $\theta \in [0, 1]$. In the following, we call this scheme FD1. We should have put a combination of explicit and implicit terms in the derivatives as well, but this leads to solving a linear system to find ρ_s , and we want to avoid that because we lose the simplicity of the approach. Let us remark, moreover, that considering the scheme

$$\begin{aligned} & \frac{\rho_{s,m}^{n+1} - \rho_{s,m}^n}{\Delta t} - (1 - \theta)\Delta_m \left(\varphi^n, \frac{\rho_s^n}{\varphi^n} \right) - \theta\Delta_m \left(\varphi^{n+1}, \frac{\rho_s^{n+1}}{\varphi^{n+1}} \right) \\ & = S((1 - \theta)\rho_{s,m}^n + \theta\rho_{s,m}^{n+1}, c_m^{n+1}) \end{aligned}$$

leads us to solve a nonsymmetric linear system, while the finite element matrices are symmetric.

A second semi-implicit approximation, which we call FD2, is the following:

$$(3.29) \quad \begin{cases} \frac{\rho_{s,m}^{n+1} - \rho_{s,m}^n}{\Delta t} - \Delta_m \left(\varphi^n, \frac{\rho_s^n}{\varphi^n} \right) = \frac{1}{2} [S(\rho_{s,m}^n, c_m^{n+1}) + S(\rho_{s,m}^{n+1}, c_m^n)], \\ \frac{c_m^{n+1} - c_m^n}{\Delta t} = \frac{1}{2} [S(\rho_{s,m}^n, c_m^{n+1}) + S(\rho_{s,m}^{n+1}, c_m^n)]. \end{cases}$$

Because the source term is quadratic, this scheme has an explicit representation:

$$(3.30) \quad \begin{cases} \frac{\rho_{s,m}^{n+1} - \rho_{s,m}^n}{\Delta t} = \frac{S(\rho_{s,m}^n, c_m^n)}{\delta} + \left(1 - \Delta t \frac{c_m^n}{2\delta}\right) \Delta_m \left(\varphi^n, \frac{\rho_s^n}{\varphi^n} \right), \\ \frac{c_m^{n+1} - c_m^n}{\Delta t} = \frac{S(\rho_{s,m}^n, c_m^n)}{\delta} - \Delta t \frac{c_m^n}{2\delta} \Delta_m \left(\varphi^n, \frac{\rho_s^n}{\varphi^n} \right) \end{cases}$$

with $\delta = 1 + \frac{\Delta t}{2} (c_m^n + \rho_{s,m}^n)$.

This discretization takes the interaction into account in a symmetric way, without computational cost. Notice also that for the single equation $y' = y^2$, the scheme $y^{n+1} = y^n + \Delta t y^{n+1} y^n$ is exact:

$$y^{n+1} = \frac{y^n}{1 - \Delta t y^n}.$$

Finally, we construct another scheme by remarking that

$$\Delta_m \left(\varphi, \frac{\rho_s}{\varphi} \right) = \Delta_m (1, \rho_s) - \frac{1}{2\Delta x} \left[\left(\frac{\rho_{s,i}}{\varphi_i} + \frac{\rho_{s,i+1}}{\varphi_{i+1}} \right) \frac{\varphi_{i+1} - \varphi_i}{\Delta x} - \left(\frac{\rho_{s,i-1}}{\varphi_{i-1}} + \frac{\rho_{s,i}}{\varphi_i} \right) \frac{\varphi_i - \varphi_{i-1}}{\Delta x} \right].$$

This is a consistent centered approximation of $\partial_x(\varphi \partial_x \frac{\rho_s}{\varphi}) = \partial_{xx} \rho_s - \partial_x(\frac{\rho_s}{\varphi} \partial_x \varphi)$.

More generally, we can put system (3.26) under the semiconservative form,

$$(3.31) \quad \begin{cases} \partial_t \rho_s + f(\rho_s, c, x, t)_x = B(\rho_s, c)_{xx} + S(\rho_s, c), \\ \partial_t c = S(c, \rho_s), \end{cases}$$

where

$$B(\rho_s, c) = \rho_s, \quad f(\rho_s, c, x, t) = \rho_s \frac{\varphi'(c)}{\varphi(c)} c_x.$$

In the expression of f , c_x is considered as a known function of (x, t) . In practice, a difference formula is used to compute it. Hence in what follows we no longer mention the (x, t) dependence in f . Let us denote $\mathbf{f} = (f, 0)$, $\mathbf{B} = (B, 0)$, $\mathbf{S} = (S, S)$. System (3.31) can be written as

$$(3.32) \quad \partial_t u + \mathbf{f}(u)_x = \mathbf{B}(u)_{xx} + \mathbf{S}(u).$$

Now the convective part may be approximated by any method for conservation law. The particular form of our system allows the flux vector splitting,

$$\mathbf{f}(u) = \mathbf{f}_+(u) - \mathbf{f}_-(u),$$

where $sp(\partial_u \mathbf{f}_\pm(u)) \subset [0, +\infty[$ and $\partial_u \mathbf{f}(u)$, $\partial_u \mathbf{f}_+(u)$ and $\partial_u \mathbf{f}_-(u)$ have a common basis of eigenvectors. In fact we have

$$\partial_u \mathbf{f} = \begin{pmatrix} \partial_{\rho_s} f & \partial_c f \\ 0 & 0 \end{pmatrix},$$

and it is sufficient to take

$$\mathbf{f}_+(u) = \begin{pmatrix} f_+(u) \\ 0 \end{pmatrix}, \quad \mathbf{f}_-(u) = \begin{pmatrix} f_-(u) \\ 0 \end{pmatrix},$$

where

$$f_+(u) = \begin{cases} f(u) & \text{if } \partial_{\rho_s} f(u) > 0, \\ 0 & \text{else} \end{cases} \quad \text{and} \quad f_-(u) = \begin{cases} -f(u) & \text{if } \partial_{\rho_s} f(u) < 0, \\ 0 & \text{else.} \end{cases}$$

Now, we can take the source term into account either like in FD1 or like in FD2. For example, let us take the same method as for FD1. The numerical scheme FD3 is the following:

$$(3.33) \quad \begin{cases} \rho_{s,m}^{n+1} = \rho_{s,m}^n - \lambda [-f_-(u_{m+1}^n) + f_+(u_m^n) + f_-(u_m^n) - f_+(u_{m-1}^n)] \\ \quad + \mu [\rho_{s,m-1}^n - 2\rho_{s,m}^n + \rho_{s,m+1}^n] + \Delta t S((1-\theta)\rho_{s,m}^n + \theta\rho_{s,m}^{n+1}, c_m^{n+1}), \\ c_m^{n+1} = c_m^n e^{-\Delta t \rho_{s,m}^n}. \end{cases}$$

To take into account the initial and boundary conditions in each of these numerical schemes, we put

$$(3.34) \quad \begin{cases} \rho_{s,m}^0 = 0, & c_m^0 = c_0 & \text{for } 1 \leq m \leq N, \\ \rho_{s,0}^n = \rho_{s0}, & \rho_{s,N+1}^n = \rho_{s,N}^n & \text{for } n \geq 0. \end{cases}$$

In the following, if $\rho_{s,m} \geq 0$, we take

$$(3.35) \quad f_{\pm}(u_m) = \rho_{s,m} \left[\pm \frac{\varphi_{m+1} - \varphi_{m-1}}{2\varphi_m \Delta x} \right]_+.$$

3.2.2. Higher order in time. To reach higher order in time for these three schemes, we remark that they all can be written in the conservative form:

$$\frac{u_m^{n+1} - u_m^n}{\Delta t} = G_m(u^{n+1}, u^n, \Delta t).$$

Moreover, when Δt tends to zero and u^n and Δx are fixed, u^{n+1} tends to u^n , and $G_m(u^{n+1}, u^n, \Delta t)$ has a limit $F_m(u^n)$. We obtain the semidiscretized scheme:

$$\mathbf{u}'_m(t_n) = F_m(\mathbf{u}(t_n)), \quad m = 1, \dots, N.$$

For FD1 and FD2, F_m is defined by

$$F_m(\mathbf{u}) = \left(\Delta_m \left(\varphi(\mathbf{c}), \frac{\rho_s}{\varphi(\mathbf{c})} \right) + \mathbf{S}(\mathbf{u}), \mathbf{S}(\mathbf{u}) \right).$$

For FD3, F_m is defined by

$$F_m(\mathbf{u}) = (\bar{\Delta}_m + \mathbf{S}(\mathbf{u}), \mathbf{S}(\mathbf{u}))$$

with

$$\bar{\Delta}_m = \frac{-f_-(u_{m+1}) + f_+(u_m) + f_-(u_m) - f_+(u_{m-1})}{\Delta x} + \frac{\rho_{s,m-1} - 2\rho_{s,m} + \rho_{s,m+1}}{\Delta x^2}.$$

This is a new starting point at which to apply a temporal scheme, solving on $[t_n, t_{n+1}]$ the ordinary differential system:

$$\mathbf{u}'(t) = F(\mathbf{u}(t)).$$

As a particular case, we may use an implicit method in order to have a large time step, and this involves the resolution of a nonlinear system. As we already have an implicit scheme with the finite element method, we prefer here to approximate u by

means of the second order Heun method or by the optimal third order strong-stability preserving (SSP) Runge–Kutta (RK) method given by

$$(3.36) \quad \begin{aligned} v^{(1)} &= u^n + \Delta t F(u^n), \\ v^{(2)} &= \frac{3}{4}u^n + \frac{1}{4}v^{(1)} + \frac{1}{4}\Delta t F(v^{(1)}), \\ u^{n+1} &= \frac{1}{3}u^n + \frac{2}{3}v^{(2)} + \frac{2}{3}\Delta t F(v^{(2)}) \end{aligned}$$

introduced in [11].

3.2.3. Stability. The finite difference schemes FD1, FD3 preserve positivity under a suitable time step restriction.

The choice of the third order RK scheme (3.36) was dictated by further stability consideration. In fact, as shown by Gottlieb, Shu, and Tadmor in [11], it is possible to relate the CFL condition for the temporal first order Euler scheme (3.33) to a strong stability property verified by the temporal third order scheme (3.36), at least for conservation laws. The rigorous extension of this property to the present case is beyond the aims of this paper, but we can expect that this scheme works for the same Δt used in the Euler time discretization, thanks to the dissipation induced by the diffusion and by the source terms.

PROPOSITION 3.3 (scheme FD1). *For all $n \geq 0$, all $m = 1, \dots, N$,*

$$(3.37) \quad \rho_{s,m}^n \geq 0, \quad c_m^n \in [0, c_0]$$

under the time step restriction

$$(3.38) \quad \Delta t \leq \frac{\beta \Delta x^2}{\varphi_0 + \beta(1 + \Delta x^2 c_0(1 - \theta))}.$$

Proof. It is clear that we have to check only the first order in time. From the expression of c_m^{n+1} , it is clear that if $\rho_{s,m}^n$ is nonnegative, then $c_m^{n+1} \in [0, c_m^n]$. This is true for $n = 0$. Let us suppose it is true for all $k \leq n$. Then $c_m^{n+1} \in [0, c_0]$ and

$$(3.39) \quad \beta \leq \varphi_m^n \leq \varphi_0.$$

Now we can write

$$(3.40) \quad \begin{aligned} \rho_{s,m}^{n+1}(1 + \Delta t \theta c_m^{n+1}) &= \rho_{s,m}^n \left[1 - \mu \left(1 + \frac{\varphi_{m+1}^n + \varphi_{m-1}^n}{2\varphi_m^n} \right) - \Delta t(1 - \theta)c_m^{n+1} \right] \\ &+ \mu \rho_{s,m-1}^n \frac{\varphi_m^n + \varphi_{m-1}^n}{2\varphi_{m-1}^n} + \mu \rho_{s,m+1}^n \frac{\varphi_m^n + \varphi_{m+1}^n}{2\varphi_{m+1}^n}. \end{aligned}$$

Thus, positivity is ensured as soon as condition (3.38) is satisfied.

PROPOSITION 3.4 (scheme FD3 with (3.35)). *For all $n \geq 0$, all $m = 1, \dots, N$,*

$$(3.41) \quad \rho_{s,m}^n \geq 0, \quad c_m^n \in [0, c_0]$$

under the time step restriction

$$(3.42) \quad \Delta t \leq \frac{2\beta \Delta x^2}{\varphi_0 + \beta(3 + 2\Delta x^2(1 - \theta))}.$$

Proof. In view of (3.35) we can write

$$\begin{aligned}
 \rho_{s,m}^{n+1}(1 + \Delta t \theta c_m^{n+1}) &= \rho_{s,m}^n \left[1 - \mu \left(\left| \frac{\varphi_{m+1} - \varphi_{m-1}}{2\varphi_m} \right| + 2 + \Delta x^2(1 - \theta)c_m^{n+1} \right) \right] \\
 &+ \rho_{s,m-1}^n (\lambda[\partial_{\rho_s} f(u_{m-1})]_+ + \mu) \\
 (3.43) \qquad &+ \rho_{s,m+1}^n (\lambda[-\partial_{\rho_s} f(u_{m+1})]_+ + \mu),
 \end{aligned}$$

and condition (3.42) follows by a straightforward computation.

Remark 3.2. In practice, we update Δt at each time step, and we use a less restrictive condition. More precisely, we require that in (3.40) or (3.43), for all $m = 1, \dots, N$, the coefficient of $\rho_{s,m}^n$ is nonnegative. By bounding c_m^{n+1} by c_m^n we use the numerical condition

$$\Delta t_n \leq \frac{\Delta x^2}{\max_{1 \leq m \leq N} \left[1 + \frac{\varphi_{m+1}^n + \varphi_{m-1}^n}{2\varphi_m^n} + \Delta x^2(1 - \theta)c_m^n \right]}$$

instead of condition (3.38). Similarly, instead of condition (3.42) we impose that

$$\Delta t_n \leq \frac{\Delta x^2}{\max_{1 \leq m \leq N} \left[\left| \frac{\varphi_{m+1}^n - \varphi_{m-1}^n}{2\varphi_m^n} \right| + 2 + \Delta x^2(1 - \theta)c_m^n \right]}.$$

4. Numerical experiments. This section is devoted to some numerical experiments. It is more significant to perform our tests on the original unscaled model (2.15)–(2.16), even if we observe that with the change of variable (2.17) the shape of the solutions is not dependent on the given parameters. The data are fixed as follows:

$$(4.1) \quad \rho_{s0} = 1, \quad c_0 = 10, \quad \alpha = 0.01, \quad \beta = 0.1, \quad m_c = 100.09, \quad m_s = 64.06, \quad d = 1.$$

As shown in section 5, letting A go to infinity is equivalent to making the time go to infinity. First we take $A = 1$ and the final time $T_{\max} = 0.1$; the last paragraph of this section and section 5 are devoted to time asymptotics.

For $\theta = 1$ and $\theta = 0.5$, let us analyze the numerical order of accuracy γ defined by

$$\gamma = \log_2 \left(\frac{\|\rho(h) - \rho(h/2)\|_1}{\|\rho(h/2) - \rho(h/4)\|_1} \right)$$

for each component of the solution at the final time T_{\max} . Here, $h = \Delta x$. We recall that schemes FD1 and FD3 are obtained by solving exactly the equation for c , and FD2 is obtained by a semi-implicit method. We call FD4 the scheme obtained by the same spatial discretization as for FD3, while the temporal resolution is the same semi-implicit one as FD2.

We first put $\theta = 1$ and for FE, $\eta^{n+1} = \eta^{n+1/2}$. As there is no upper bound on Δt for the finite element method in this case, we have chosen $\Delta t = \Delta x$. The scheme is first order in time. We do not experiment with FD2 and FD4 here, because they correspond to $\theta = 1/2$. We obtain Tables 1–3.

Scheme FD1, that is, when the nonlinear diffusion is approximated by formula (3.27), converges better than scheme FD3. For the finite element case, the choice of a large time step prevents one from a fast convergence. Nevertheless, the convergence

TABLE 1
The L^1 errors for FD1, $\theta = 1$.

h	γ_s	$\ \rho_s(h) - \rho_s(h/2)\ _1$	γ_c	$\ c(h) - c(h/2)\ _1$
0.2	0.312985829	0.00834144243	1.87384348	0.000525266
0.1	2.40471333	0.00671464464	1.3467364	0.0001433165
0.05	1.33397634	0.00126803776	1.49975333	5.634925E-05
0.025	2.2831098	0.000502996885	3.1590019	1.9925875E-05
0.0125	1.67597534	0.000103342928	0.83185905	2.2308125E-06
0.00625	3.29717645	3.23416303E-05	4.7235384	1.25328125E-06
0.003125	—	3.29012875E-06	—	4.74375001E-08

TABLE 2
The L^1 errors for FD3, $\theta = 1$.

h	γ_s	$\ \rho_s(h) - \rho_s(h/2)\ _1$	γ_c	$\ c(h) - c(h/2)\ _1$
0.2	1.58822799	0.045138069	2.35937874	0.000867266
0.1	0.215780607	0.0150120053	-0.396735465	0.0001690085
0.05	0.981610986	0.0129265394	1.01033173	0.000222504
0.025	1.13931055	0.00654617968	1.29691797	0.000110458125
0.0125	0.908544914	0.00297181158	0.833852008	4.4955875E-05
0.00625	1.02937252	0.00158314976	1.06622513	2.52215625E-05
0.003125	—	0.000775621775	—	1.20449844E-05

TABLE 3
The L^1 errors for the finite element method, $\theta = 1$.

h	γ_s	$\ \rho_s(h) - \rho_s(h/2)\ _1$	γ_c	$\ c(h) - c(h/2)\ _1$
0.2	-2.25922932	0.00487514386	—	0.
0.1	-0.71418536	0.023339053	3.10173338	0.001743642
0.05	-0.991921129	0.0382890373	-3.52219246	0.00020311525
0.025	1.33297029	0.0761504476	1.61661945	0.00233360913
0.0125	2.08378342	0.0302279307	1.38231411	0.000760986875
0.00625	-0.343775269	0.00713061687	-0.138516672	0.000291916844
0.003125	—	0.00904927466	—	0.000321334109

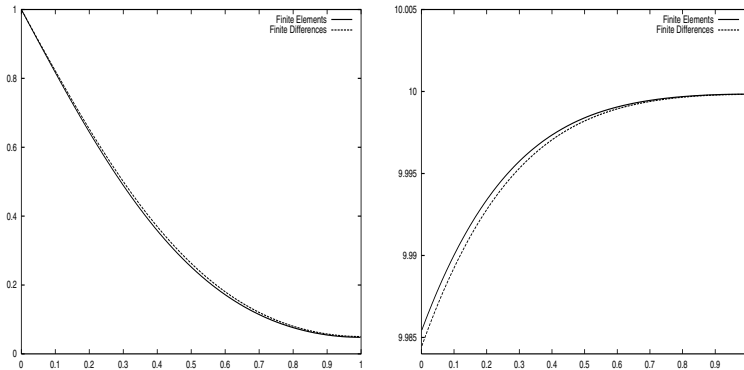


FIG. 1. Comparison among finite element methods and finite difference methods, with $\Delta x = 0.003125$ and $\theta = 1$. Left: SO₂ concentration; right: calcite density. Time $t = 0.1$.

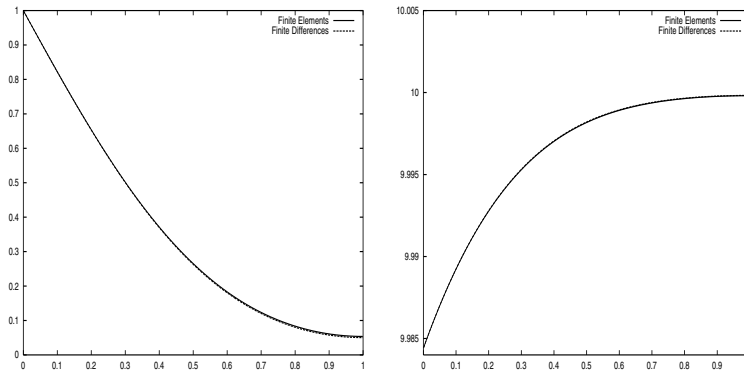


FIG. 2. Comparison among finite element methods and finite difference methods, with $\Delta x = 0.0015625$ and $\theta = 1$. Left: SO_2 concentration; right: calcite density. Time $t = 0.1$.

TABLE 4
The L^1 errors for FD1, $\theta = 1/2$.

h	γ_s	$\ \rho_s(h) - \rho_s(h/2)\ _1$	γ_c	$\ c(h) - c(h/2)\ _1$
0.2	1.17222647	0.0084354273	3.36048996	0.000529403
0.1	2.00077673	0.00374310282	2.001092	5.1544E-05
0.05	2.0139494	0.000935272028	2.0079489	1.287625E-05
0.025	2.0292682	0.000231568118	2.01466401	3.201375E-06
0.0125	2.05711582	5.67293969E-05	2.03945881	7.9225E-07
0.00625	2.09897113	1.36318438E-05	2.04442335	1.9271875E-07
0.003125	—	3.18200844E-06	—	4.67187501E-08

TABLE 5
The L^1 errors for FD2, $\theta = 1/2$.

h	γ_s	$\ \rho_s(h) - \rho_s(h/2)\ _1$	γ_c	$\ c(h) - c(h/2)\ _1$
0.2	1.17179262	0.00843434345	1.12743968	0.000263196
0.1	2.0006973	0.00374374754	2.01027543	0.000120472
0.05	2.01389756	0.00093548462	2.00610367	2.990425E-05
0.025	2.02923763	0.000231629077	2.00869842	7.4445E-06
0.0125	2.05709045	5.67455331E-05	2.01474625	1.8499375E-06
0.00625	2.09895461	1.36359609E-05	2.03115964	4.5778125E-07
0.003125	—	3.18300594E-06	—	1.12E-07

holds, and as shown in Figures 1 and 2, the solution is close to the one computed by FD1. Let us point out that a computation for $\Delta x = 0.0015625$ and $\Delta t = \Delta x$ is much faster than a computation for $\Delta x = 0.00625$ and $\Delta t = C\Delta x^2$.

Let us now make the same experiment with $\theta = 1/2$. In that case, for the finite element method, we choose the Heun method for η^{n+1} with formula (3.14). Tables 4–8 show that numerically FD1, FD2, and FE-1/2 are second order accurate, while FD3 and FD4 remain less than first order accurate. Let us recall that unless a is a constant, the formula (3.27) used in FD1 and FD2 is only first order in space, and that for FD1 the choice of θ affects only the source term and not the diffusion term. Therefore, second order was not expected. This result can be explained by the fact that here the variations of c and $a = \varphi(c)$ are small in space and in time; see Figure 1, for example. On the contrary, the semiconservative formulation (3.31) used to construct schemes FD3 and FD4 does not allow such a gain.

TABLE 6
The L^1 errors for FD3, $\theta = 1/2$.

h	γ_s	$\ \rho_s(h) - \rho_s(h/2)\ _1$	γ_c	$\ c(h) - c(h/2)\ _1$
0.2	1.33149717	0.0452259789	1.7650704	0.000870125
0.1	0.743923424	0.0179707991	0.686674157	0.0002560015
0.05	0.884689522	0.0107306029	0.850347453	0.00015904975
0.025	0.945292297	0.00581173816	0.926766823	8.8217125E-05
0.0125	0.973358008	0.00301817698	0.963707356	4.6405375E-05
0.00625	0.986854034	0.00153721547	0.98201168	2.37937813E-05
0.003125	—	0.00077564336	—	1.20461563E-05

TABLE 7
The L^1 errors for FD4, $\theta = 1/2$.

h	γ_s	$\ \rho_s(h) - \rho_s(h/2)\ _1$	γ_c	$\ c(h) - c(h/2)\ _1$
0.2	1.33151869	0.0452259099	1.79104267	0.000677384
0.1	0.743919588	0.0179705035	0.453029589	0.000195739
0.05	0.884682254	0.0107304549	0.766586208	0.00014298875
0.025	0.945286757	0.00581168729	0.890333851	8.404975E-05
0.0125	0.973354679	0.00301816215	0.946713033	4.53439375E-05
0.00625	0.986852184	0.00153721146	0.973711741	2.35250312E-05
0.003125	—	0.000775642332	—	1.19788125E-05

TABLE 8
The L^1 errors for finite element, $\theta = 1/2$.

h	γ_s	$\ \rho_s(h) - \rho_s(h/2)\ _1$	γ_c	$\ c(h) - c(h/2)\ _1$
0.2	3.50066927	0.0545620474	6.44459105	0.001924897
0.1	1.99293298	0.00482041247	1.99127884	2.21E-05
0.05	2.00834819	0.00121102077	2.01460837	5.5585E-06
0.025	2.02053637	0.000301008351	2.03328576	1.375625E-06
0.0125	2.03989415	7.41884825E-05	2.07065766	3.360625E-07
0.00625	2.0685759	1.80412722E-05	2.14077583	8.E-08
0.003125	—	4.30094375E-06	—	1.8140625E-08

TABLE 9
The L^1 errors for FD1, $\theta = 1/2$, order 3 in time.

h	γ_s	$\ \rho_s(h) - \rho_s(h/2)\ _1$	γ_c	$\ c(h) - c(h/2)\ _1$
0.2	2.34357642	0.0132414991	2.19330999	0.000390955
0.1	1.99675824	0.00260885747	2.01397425	8.5482E-05
0.05	2.01399821	0.000653681548	2.00827172	2.11645E-05
0.025	2.03298887	0.000161842415	2.0117367	5.260875E-06
0.0125	2.0516014	3.95459231E-05	2.02235917	1.3045625E-06
0.00625	2.05713482	9.53911656E-06	2.0462204	3.21125E-07
0.003125	—	2.29218078E-06	—	7.775E-08

TABLE 10
The L^1 errors for FD2, $\theta = 1/2$, order 3 in time.

h	γ_s	$\ \rho_s(h) - \rho_s(h/2)\ _1$	γ_c	$\ c(h) - c(h/2)\ _1$
0.2	2.3431196	0.0132405316	-0.16126272	0.000139208
0.1	1.99663095	0.00260949301	2.01341207	0.0001556715
0.05	2.01393858	0.000653898483	2.00595212	3.855775E-05
0.025	2.03295263	0.000161902817	2.00708072	9.59975E-06
0.0125	2.05161953	3.95616763E-05	2.01087687	2.3881875E-06
0.00625	2.05719473	9.54279656E-06	2.02687804	5.925625E-07
0.003125	—	2.29296984E-06	—	1.4540625E-07

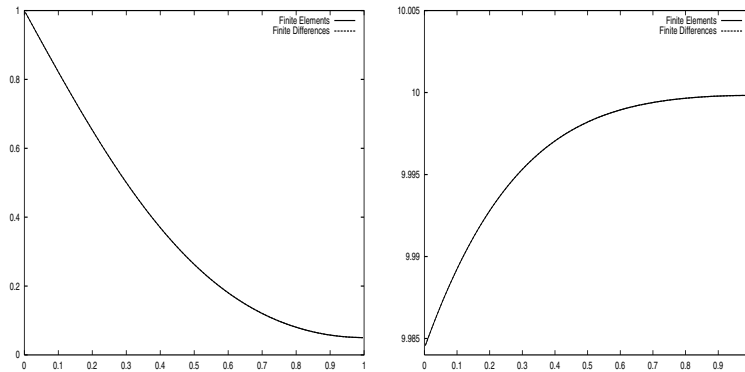


FIG. 3. Comparison among finite element methods and finite difference methods, with $\Delta x = 0.00625$ and $\theta = 0.5$. Left: SO_2 concentration; right: calcite density. Time $t = 0.1$.

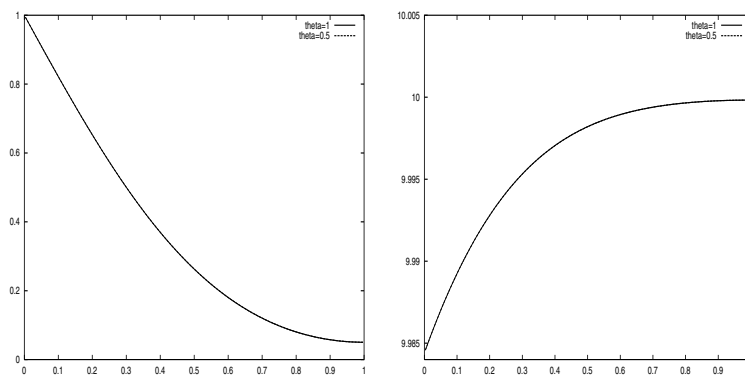


FIG. 4. Finite differences: comparison among $\theta = 0.5$ and $\theta = 1$, with $\Delta x = 0.00625$. Left: SO_2 concentration; right: calcite density. Time $t = 0.1$.

To end this part of the tests, in Tables 9 and 10 we give the numerical order for the third order time discretization applied to FD1 and FD2. The numerical order of accuracy is not sensitive to time order increasing, but the error $\|u(h) - u(h/2)\|_1$ is smaller. This is not surprising, since the spatial discretization remains unchanged. We do not present graphical results for high order in time discretizations because in all our experiments they coincide with what happens for first order. Taking into account that high time order makes the computation longer, we conclude that one should prefer first order schemes.

To complete these tests, we present some graphical results. In Figure 1, we compare the results for finite element and finite difference FD1 methods, for $\theta = 1$ and $\Delta x = 0.003125$. Then in Figure 2 we make the same comparison for $\Delta x = 0.0015625$, where both results coincide. In Figure 3 we show that for $\theta = 0.5$ finite element and finite difference FD1 methods give very similar results for $\Delta x = 0.00625$. This is because in this case both time steps are comparable, while for $\theta = 1$ we take $\Delta t = \Delta x$ in the finite element method. Hence, the figures confirm the observations made in the tables. We also remark that for finite difference method FD1, the results do not depend on the value of θ ; see Figure 4. All these results are computed at time $t = 0.1$.

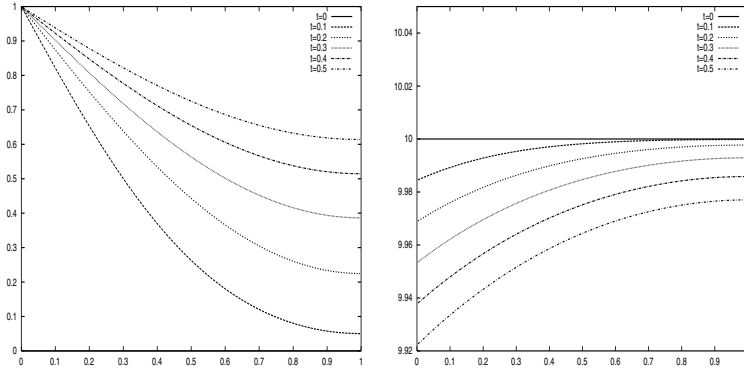


FIG. 5. Solution from $t = 0$ to $t = 0.5$ with $A = 1$. Left: SO_2 concentration; right: calcite density.

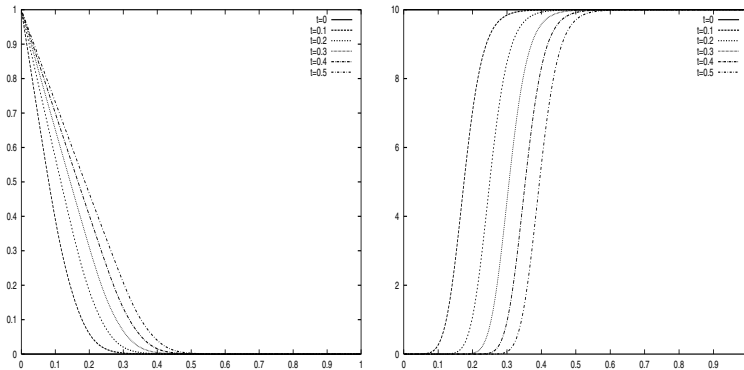


FIG. 6. Solution from $t = 0$ to $t = 0.5$ with $A = 10000$. Left: SO_2 concentration; right: calcite density.

From now on, we take $\theta = 0.5$, and we use the finite difference method FD1. Figure 5 shows the solution for different times, from $t = 0$ to $t = 0.5$, with $A = 1$.

Finally, we put $A = 10000$, and we plot the solution from $t = 0$ to $t = 0.5$ (Figure 6). The solution has a very different qualitative aspect: the transition zone is smaller as the interaction coefficient A increases, so that the calcite deterioration is more important for the boundary of the sample, while the interior is not touched by SO_2 . The next section is devoted to the study of such solutions.

5. Qualitative behavior of the solutions. In this section we discuss, by means of a formal scaling, the qualitative behavior of the solutions for large times, and we give a numerical verification of this asymptotics. These results will be very useful in calibrating our model against experimental tests.

5.1. A scaling argument. Let us rewrite the system in the one-dimensional case and in the scaled form

$$(5.1) \quad \begin{cases} \partial_t(\varphi(c)s) - \partial_x(\varphi(c)\partial_x s) = -\varphi(c)sc, \\ \partial_t c = -\varphi(c)sc. \end{cases}$$

For simplicity we assume that the domain is the half-line $x > 0$. Therefore we have to give the initial and boundary conditions. Here we consider the simple case of invariant data

$$(5.2) \quad s(x, 0) = 0, \quad c(x, 0) = c_0,$$

and

$$(5.3) \quad s(0, t) = \hat{s}$$

for two positive constant values c_0, \hat{s} .

Following [15], we make the scaling (kx, k^2t) in the unknowns, which yields

$$(5.4) \quad s^k(x, t) = s(kx, k^2t), \quad c^k(x, t) = c(kx, k^2t).$$

Clearly, the new unknowns satisfy the scaled problem

$$(5.5) \quad \begin{cases} \partial_t(\varphi(c)s) - \partial_x(\varphi(c)\partial_x s) = -k^2\varphi(c)sc, \\ \partial_t c = -k^2\varphi(c)sc, \end{cases}$$

with the same initial boundary conditions.

Assume now that there exists the limit of the sequence (s^k, c^k) for $k \rightarrow \infty$. Namely, there exist (S, C) , such that

$$(5.6) \quad (s^k, c^k) \rightarrow_{k \rightarrow \infty} (S, C),$$

in some suitable (strong) topology. Using the scaling properties of the sequence (s^k, c^k) , we have that (S, C) is a self-similar weak solution to the problem

$$(5.7) \quad \begin{cases} \partial_t(\varphi(C)S - C) - \partial_x(\varphi(C)\partial_x S) = 0, \\ CS = 0, \end{cases}$$

with the initial boundary conditions (5.2)–(5.3). Self-similarity is just a consequence of the definition of the limit under the scaling (kx, k^2t) . Therefore we have that we can write

$$(5.8) \quad S(x, t) = \Sigma\left(\frac{x}{\sqrt{t}}\right), \quad C(x, t) = \Gamma\left(\frac{x}{\sqrt{t}}\right),$$

where Σ, Γ are one-dimensional functions such that

$$(5.9) \quad \begin{cases} \frac{1}{2}\xi(\varphi(\Gamma)\Sigma - \Gamma)' + (\varphi(\Gamma)\Sigma')' = 0, \\ \Gamma\Sigma = 0, \end{cases}$$

and

$$(5.10) \quad \Sigma(0) = \hat{s}, \quad \lim_{\xi \rightarrow \infty} \Sigma(\xi) = 0, \quad \lim_{\xi \rightarrow \infty} \Gamma(\xi) = c_0.$$

Let us now give one explicit solution to problem (5.9)–(5.10). Since $\hat{s} > 0$, at least for small values of ξ we have that $\Sigma > 0$ and $\Gamma = 0$. Let $\xi_0 > 0$ be the supremum value of the set $\{\xi > 0 | \Sigma(\xi) > 0\}$. In the interval $(0, \xi_0)$, the function Σ satisfies

$$\frac{1}{2}\xi\Sigma' + \Sigma'' = 0,$$

which implies that, from the condition at infinity,

$$(5.11) \quad \Sigma(\xi) = \hat{s} - \alpha \int_0^\xi e^{-\frac{1}{4}\eta^2} d\eta$$

for some $\alpha > 0$. In particular, let ξ_0 be a finite value, i.e., such that $\Sigma(\xi_0) = 0$. Then, clearly,

$$(5.12) \quad \alpha = \frac{\hat{s}}{\int_0^{\xi_0} e^{-\frac{1}{4}\eta^2} d\eta}.$$

Let us continue our solution by setting $\Sigma \equiv 0$ for $\xi \geq \xi_0$. Considering the unknowns S and C , let us denote by $\zeta(t)$ the curve where $S = 0$, which is now given by the equation

$$\zeta(t) = \xi_0 \sqrt{t},$$

which gives

$$\zeta'(t) = \frac{\xi_0}{2\sqrt{t}}.$$

On the other side, we have to satisfy the Rankine–Hugoniot condition for the conservation law (5.9)–(5.10), which yields

$$(5.13) \quad \zeta'(t) = -\frac{(\partial_x s)(\zeta(t)-)}{c_0}.$$

Now, by equating the right-hand side in the equations we obtain

$$(5.14) \quad \alpha = \frac{\xi_0 c_0}{2} e^{\frac{1}{4}\xi_0^2}.$$

Therefore, by using (5.12), we obtain a relation for ξ_0 :

$$(5.15) \quad F(\xi_0) := \xi_0 \int_0^{\xi_0} e^{\frac{1}{4}(\xi_0^2 - \eta^2)} d\eta = \frac{2\hat{s}}{c_0}.$$

Since $F(0) = 0$ and $\lim_{\xi \rightarrow \infty} F(\xi) = \infty$ and $F' > 0$, there exists $G = F^{-1}$, the inverse function of F , and we take as ξ_0 the unique value $\xi_0 = G(\frac{2\hat{s}}{c_0})$.

Let us resume our situation. There exists a self-similar weak solution of problem (5.9)–(5.10), which is given by

$$(5.16) \quad (S(x, t), C(x, t)) = \begin{cases} S = \hat{s} - \frac{\xi_0 c_0}{2} \int_0^{\frac{x}{\sqrt{t}}} e^{\frac{1}{4}(\xi_0^2 - \eta^2)} d\eta, & C = 0, \quad x \in (0, \xi_0 \sqrt{t}), \\ S = 0, \quad C = c_0, & x > \xi_0 \sqrt{t}, \end{cases}$$

where ξ_0 is the unique solution of (5.15). If we restrict our attention to the unknown S , we find that it is just a weak solution to the one-phase Stefan problem,

$$(5.17) \quad \begin{cases} \partial_t S - \partial_{xx} S = 0 & \text{for } x \in (0, \zeta(t)), \\ S(x, 0) = 0, \\ S(\zeta(t), 0) = 0, \\ \zeta'(t) = -\frac{(\partial_x s)(\zeta(t)-)}{c_0}. \end{cases}$$

As is well known [20], this problem has a unique explicit solution. Therefore we can find that the limit problem (5.8) also has a unique self-similar weak solution.

Let us now investigate the relation between this scaling and the asymptotic behavior of the solution (s, c) to (5.1), (5.2), (5.3). Assuming the limit (5.6), we have that, fixing $t = 1$,

$$(s(kx, k^2), c(kx, k^2)) = (s^k(x, 1), c^k(x, 1)) \rightarrow (S(x, 1), C(x, 1)) \quad \text{as } k \rightarrow \infty.$$

Now, setting $y = kx$ and $\tau = k^2$, we find that

$$(5.18) \quad \left(s(y, \tau) - S\left(\frac{y}{\sqrt{\tau}}, 1\right), c(y, \tau) - C\left(\frac{y}{\sqrt{\tau}}, 1\right) \right) \rightarrow (0, 0) \quad \text{as } \tau \rightarrow \infty.$$

The rigorous proof of this result is beyond the aims of this paper and will be considered in a future work. In the following we present a consistent numerical verification of this asymptotic behavior.

5.2. A numerical study. Let us analyze numerically the asymptotic behavior of the solution. The following questions are under consideration:

- Does the approximate solution have the correct asymptotic limit?
- How does the front appear?
- What is the convergence rate to the limit?

We consider the unscaled model (2.15)–(2.16) with the previous parameters (4.1) and $A = 100$. Let us denote $g(\xi) = \int_0^\xi e^{-x^2/4} dx$. The above results read

$$\lim_{t \rightarrow +\infty} s(x, t) - \sigma\left(\frac{x}{\sqrt{t}}\right) = 0, \quad \lim_{t \rightarrow +\infty} c(x, t) - \gamma\left(\frac{x}{\sqrt{t}}\right) = 0$$

with

$$\begin{cases} \sigma(\xi) = \frac{\rho_{s0}}{\varphi(0)} \left[1 - \frac{g(\xi)}{g(\xi_0)} \right] & \text{if } \xi < \xi_0, \quad 0 \text{ otherwise,} \\ \gamma(\xi) = c_0 & \text{if } \xi > \xi_0, \quad 0 \text{ otherwise.} \end{cases}$$

Here ξ_0 is the unique solution of

$$\xi e^{\xi^2/4} g(\xi) = \frac{2\rho_{s0}m_c}{c_0m_s}.$$

By strict convexity, Newton’s method converges to solve this equation, and we find $\xi_0 = 0.545$ approximatively.

As mentioned in section 4, the fully implicit finite element method ($\theta = 1$) is the cheaper in terms of computation times, so we choose this method here. We compute the solution on a rather large space interval— $[0, 10]$ —to avoid the influence of the right boundary condition. As the front position is $x(t) = \xi_0\sqrt{t}$, this allows us to compute the solution for $t < 300$. We take $\Delta x = 0.01$ and $\frac{\Delta t}{\Delta x} = 0.5$. To make sure that this choice is correct, we first compared the solution at $t = 10$ with the one obtained by explicit finite differences with $\frac{\Delta t}{\Delta x^2} = C$. Both results coincide; see Figure 7.

Figure 8 represents early times and the formation of the front. We have $c(0, t) = c_0 e^{-At/m_s}$. This gives $c(0, 5) = 0.004$, and $10^{-7} < c(0, 10) < 10^{-6}$. In fact, after the time $t = 5$, we already observe the asymptotic profile on the calcite density.

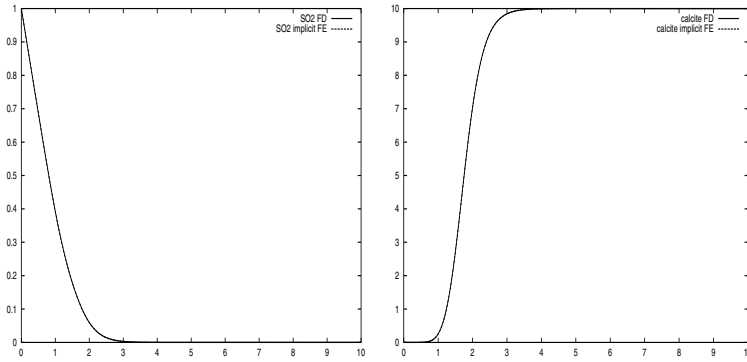


FIG. 7. Comparison among implicit finite element methods and explicit finite difference methods. Left: SO₂ concentration; right: calcite density. Time $t = 10$.

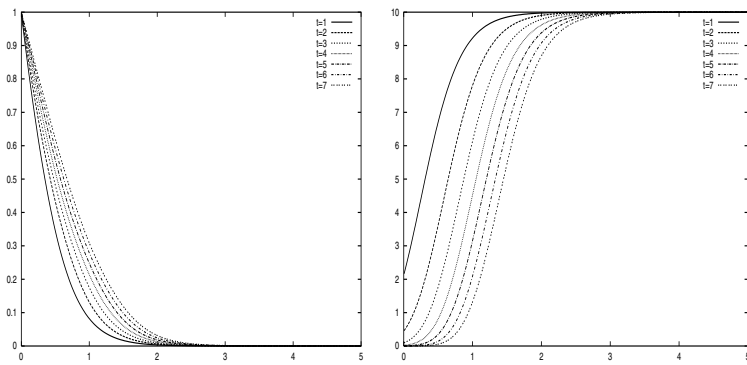


FIG. 8. Front formation. Left: SO₂ concentration; right: calcite density.

If we now compute the solution for large times and compare it to the theoretical limit, we obtain qualitatively a good agreement with our prediction, as shown in Figure 9, where we represent the solution with respect to an x/\sqrt{t} -scale, in order to observe the convergence to the asymptotic state. Let us study the convergence more carefully. As suggested by theoretical results [15], which were obtained for the case with constant porosity and constant diffusion, we expect that s converges on \mathbb{R}_x^+ while c converges out of the front. Let us denote

$$e_s(x, t) = \left| s(x, t) - \sigma \left(\frac{x}{\sqrt{t}} \right) \right|, \quad e_c(x, t) = \left| c(x, t) - \gamma \left(\frac{x}{\sqrt{t}} \right) \right|$$

and for $\delta \geq 0, t \geq 0$,

$$X(\delta, t) = \left\{ x \in \mathbb{R}^+, \left| \frac{x}{\sqrt{t}} - \xi_0 \right| \geq \delta \right\}.$$

For $p \in [1, +\infty]$, we study

$$E_s(A, p, \delta, t) = \|e_s(\cdot, t)\|_{L^p(X(\delta, t))}, \quad E_c(A, p, \delta, t) = \|e_c(\cdot, t)\|_{L^p(X(\delta, t))}.$$

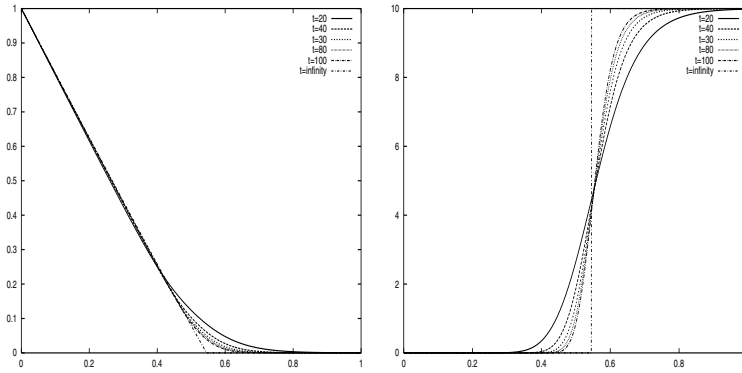


FIG. 9. Large time behavior. Left: SO_2 concentration; right: calcite density, with respect to the x/\sqrt{t} -scale.

If (s, c) is a solution of system (2.15)–(2.16) with $A = 1$, then the scaled function (s^k, c^k) defined in (5.4) is a solution of the same equations with $A = k^2$. Therefore, we have the following result.

PROPOSITION 5.1. For any $p \in [1, +\infty]$, $\delta \geq 0$, $t \geq 0$,

(5.19)

$$E_s(A, p, \delta, t) = A^{-1/2p} E_s(1, p, \delta, At), \quad E_c(A, p, \delta, t) = A^{-1/2p} E_c(1, p, \delta, At).$$

Suppose now that

$$E_s(A, p, \delta, t) = C_s(A, p, \delta) t^{-r_s}, \quad E_c(A, p, \delta, t) = C_c(A, p, \delta) t^{-r_c}.$$

Then

$$\begin{aligned} E_s(1, p, \delta, t) &= A^{r_s+1/2p} C_s(A, p, \delta) t^{-r_s}, \\ E_c(1, p, \delta, t) &= A^{r_c+1/2p} C_c(A, p, \delta) t^{-r_c}. \end{aligned}$$

Consequently, the convergence rates r_s, r_c do not depend on A . The other parameters are fixed by the physical properties of the calcite specimen and the SO_2 . From these considerations, we conclude that these convergence rates may be considered as specific to the problem. We have determined them experimentally for $p = +\infty, p = 1, p = 2$.

As far as we are concerned with uniform convergence, the results are as expected—the SO_2 concentration converges uniformly on \mathbb{R}^+ and the calcite density does not:

$$\lim_{t \rightarrow +\infty} E_s(A, \infty, 0, t) = 0, \quad \lim_{t \rightarrow +\infty} E_c(A, \infty, 0, t) \neq 0.$$

We have then computed the maximum difference between the asymptotic limit and the computed solution, out of the front, for different values of δ in the range $[0.01\xi_0, 0.2\xi_0]$. For $\delta \geq 0.05\xi_0$ we observe that

$$\lim_{t \rightarrow +\infty} E_c(A, \infty, \delta, t) = 0.$$

These results are shown in Figure 10. In the legend we denoted $d = \delta/\xi_0$. The convergence rates are shown in Figure 11. As we evaluate them at each time step,

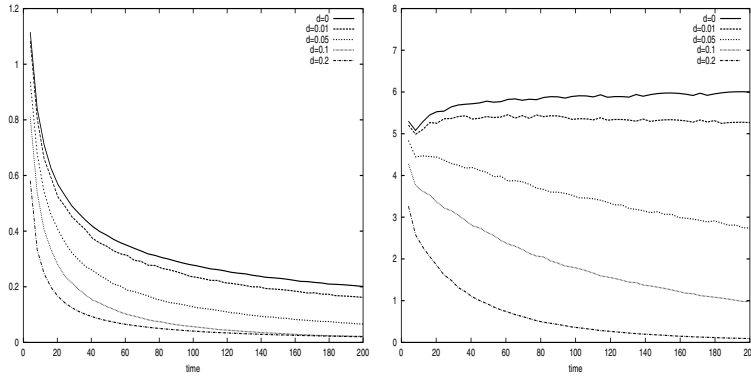


FIG. 10. Maximal distance to asymptotic solution, out of the front, with respect to time. Left: SO₂ concentration; right: calcite density.

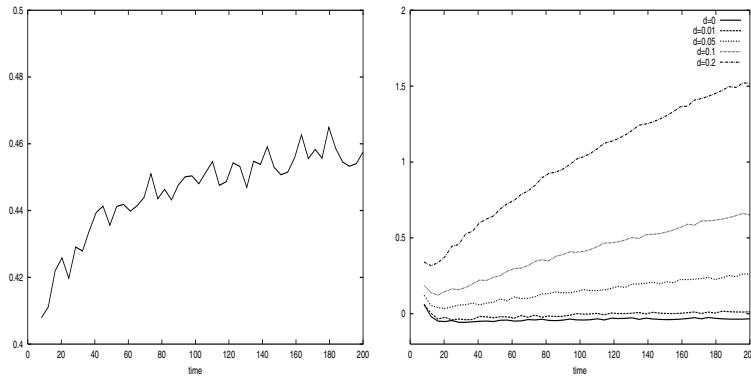


FIG. 11. Convergence rate in maximum norm, with respect to time. Left: SO₂ concentration; right: calcite density.

we obtain a function of time that is asymptotic to a constant value for large times. For SO₂, we show only the result for $\delta = 0$: we find that r_s is about 0.45. For the second variable, the convergence rate r_c is also about 0.4 for $\delta = 0.1\xi_0$. For the values considered here, it is an increasing function of δ . Observe that the rates begin to stabilize after the time $t = 5$, that is, the time for which we see the formation of the front.

The analysis of L^1 and L^2 convergences leads to similar results. In Figures 12 and 13, we represented the L^1 and L^2 distances of the computed solution to the theoretical limit, out of the front. As we already have uniform convergence of s on \mathbb{R}^+ , it is clear that s converges also in L^p norm, and we actually observe it. With regard to the calcite density, we do not find out L^1 or L^2 convergence, where uniform convergence does not hold, although the curves for $\delta = 0.01\xi_0$ are slightly decreasing. Finally, Figures 14 and 15 give the convergence rates, and they are similar to the ones for the L^∞ norm. We also remark that these numerical results are in sharp contrast to the analytical results of [16, 4], where global strong convergence, i.e., up the front, of the reactive unknown c was proven for the case $\alpha = 0$, namely, in the constant porosity case. Actually, this convergence is observed also at the numerical level by using our

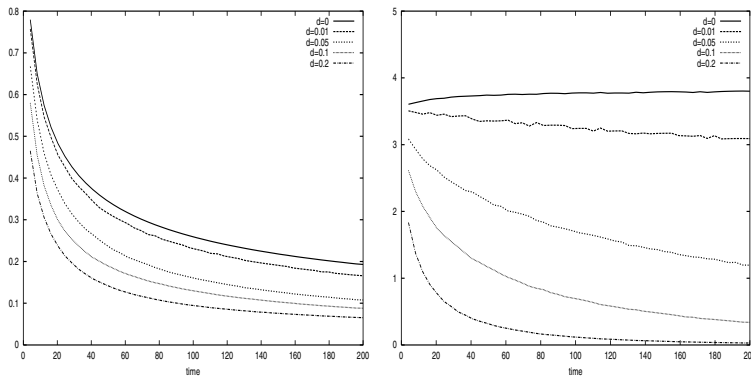


FIG. 12. L^1 distance to asymptotic solution, out of the front, with respect to time. Left: SO_2 concentration; right: calcite density.

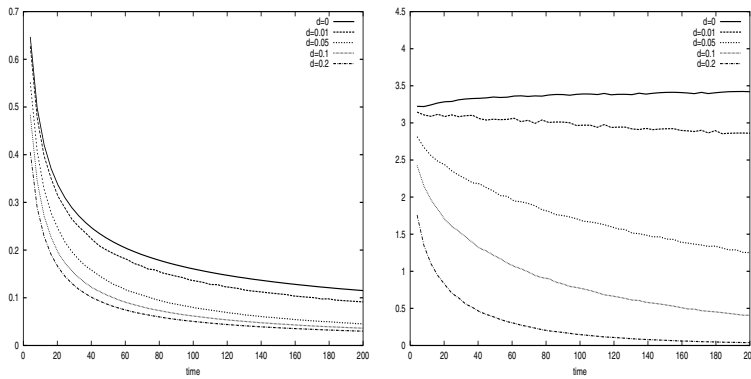


FIG. 13. L^2 distance to asymptotic solution, out of the front, with respect to time. Left: SO_2 concentration; right: calcite density.

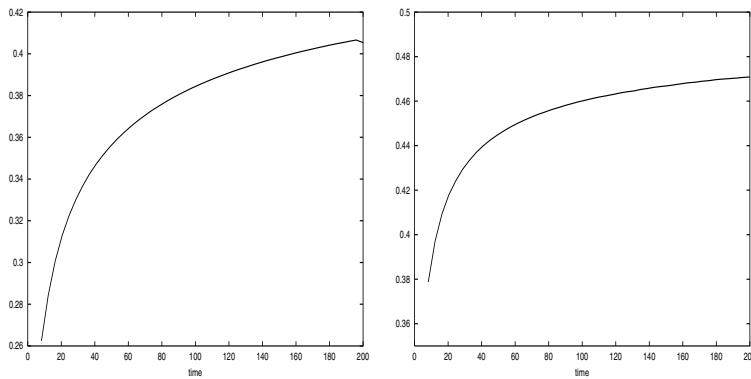


FIG. 14. L^p convergence rate for SO_2 with respect to time. Left: $p = 1$; right: $p = 2$.

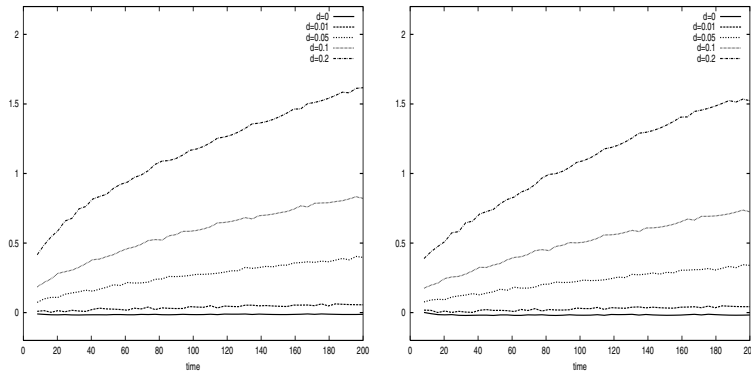


FIG. 15. L^p convergence rate out of the front for calcite with respect to time. Left: $p = 1$; right: $p = 2$.

schemes. The main difference between the constant and the nonconstant porosity case is in the singular nonlinear term $\alpha c_x s_x$, which appears in the nonconstant case by developing all the derivatives in (1.1). Actually, this is the main difficulty toward obtaining a rigorous proof of (5.18).

5.3. Comparison with experimental results. The asymptotic profile (5.16) of our solutions shows that there exists a clear front of gypsum, which evolves as a linear function of \sqrt{t} . Let us notice here that this behavior has been experimentally observed in many independent tests; see, for instance, [22, 23, 7, 8, 17]. In connection with the present research, some new laboratory tests were performed in [10], and great care was given to force the monoaxial symmetry of the experiment and to establish a clear dependence of the speed of the front on the physical parameters.

Figure 16 presents on the left the numerical simulation of the evolution of the front, plotted as a function of \sqrt{t} , while the right presents the gypsum thickness values at different times, in the same scale, as given by the preliminary experimental results given in [10].

It is possible to observe a good qualitative agreement between the numerical

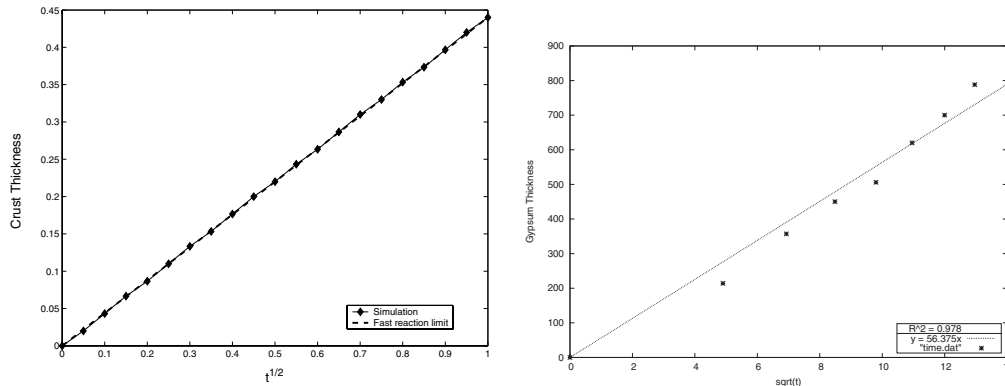


FIG. 16. Left: Position of the calcite front as a function of \sqrt{t} . The simulated results were obtained using 300 finite elements, $\Delta t = 1/3000$, and $k = 10^5$. Right: Crust thickness measured in function of time reaction as obtained in the laboratory test in [10].

prediction and the experimental data, which gives the possibility of a future calibration of the parameters on a larger set of data. In this way it will be possible to quantify the real damage phenomena on the stone materials.

6. Conclusion. We have considered a macroscopic hydrodynamic model for the evolution of the gypsum fronts in calcium carbonate stones, for which we have designed several finite element and finite difference discretizations. The finite element method involves the resolution of one tridiagonal linear system per time step. All the finite difference schemes have an explicit formulation and allow high order in time, but we have noticed that in our context, first order seems to be sufficient.

Our numerical experiments show that the approximations FD3 and FD4 are less efficient than the others. An interesting feature of the methods FE, FD1, and FD2 with $\theta = 1/2$ is that for short times they are numerically second order accurate. We have also observed that the implicit finite element method FE-1 can be used with a hyperbolic like time step $\Delta t = C.\Delta x$, which allows fast computations.

Numerical stability is established, and all those schemes give comparable shapes. We have produced asymptotic solutions for the model, and they are retrieved by the computational results. Moreover, this behavior is in qualitative agreement with the experimental tests. This is an important step in the validation of the model. In view of these encouraging facts, multidimensional computations on realistic complex geometries are now under consideration.

Acknowledgments. The authors would like to thank G. I. Barenblatt for valuable discussions about this work. We thank Rein van der Hout, Gianni Royer, Carlo Nitsch, and Maria Laura Santarelli, who read the first version of this manuscript and made many interesting remarks. We also thank Micaela Incitti and Vidar Furuholt for their active collaboration.

REFERENCES

- [1] G. ALÌ, V. FURUHOLT, R. NATALINI, AND I. TORCICOLLO, *Numerical and Qualitative Analysis of a Mathematical Model of Sulphate Chemical Aggression of Limestones with High Permeability*, IAC report, Istituto per le Applicazioni del Calcolo “Mauro Picone,” Rome, Italy, 2004. Available online at <http://www.iac.rm.cnr.it/~natalini/ps/afnt.pdf>.
- [2] G. G. AMOROSO AND V. FASSINA, *Stone Decay and Conservation—Atmospheric Pollution, Cleaning, Consolidation and Protection*, Elsevier, Amsterdam, 1983.
- [3] G. I. BARENBLATT, V. M. ENTONOV, AND V. M. RYZHIK, *Theory of Fluid Flows through Natural Rocks*, Kluwer Academic Publishers, Dordrecht, The Netherlands, 1990.
- [4] M. BELHADJ, J.-F. GERBEAU, AND B. PERTHAME, *A multiscale colloid transport model with anisotropic degenerate diffusion*, *Asymptot. Anal.*, 34 (2003), pp. 41–54.
- [5] R. BUGINI, M. LAURENZI TABASSO, AND M. REALINI, *Rate of formation of black crusts on marble. A case study*, *J. Cultural Heritage*, 1 (2000), pp. 111–116.
- [6] F. GARBASSI, E. MELLO, AND M. LAURENZI TABASSO, *In situ XPS observation of the first stages of marble sulphation by atmospheric SO₂*, *Durability Build. Mater.*, 3 (1985), pp. 51–58.
- [7] K. L. GAURI AND J. A. GWINN, *Deterioration of marble in air containing 5–10 ppm SO₂ and NO₂*, *Durability Build. Mater.*, 1 (1982/83), pp. 217–223.
- [8] K. L. GAURI, N. P. KULSHRESHTHA, A. R. PUNURU, AND A. N. CHOWDHURY, *Rate of decay of marble in laboratory and outdoor exposure*, *J. Mater. Civil Engrg.*, 1 (1989), pp. 73–85.
- [9] K. L. GAURI, R. POPLI, AND A. C. SARMA, *Effect of relative humidity and grain size on the reaction rates of marble at high concentrations of SO₂*, *Durability Build. Mater.*, 1 (1982/83), pp. 209–216.
- [10] C. GHAVARINI, M. INCITTI, M. L. SANTARELLI, R. NATALINI, AND V. FURUHOLT, *A Non-linear Model of Sulphation of Calcium Carbonate Stones: Numerical Simulations and Preliminary Laboratory Assessments*, IAC report 19, Istituto per le Applicazioni del

- Calcolo “Mauro Picone,” Rome, Italy, 2003. Available online at <http://www.iac.rm.cnr.it/~natalini/ps/C1pre.pdf>.
- [11] S. GOTTLIEB, C.-W. SHU, AND E. TADMOR, *Strong stability-preserving high-order time discretization methods*, SIAM Rev., 43 (2001), pp. 89–112.
 - [12] F. R. GUARGUAGLINI AND R. NATALINI, *Global Existence of Smooth Solutions to a Nonlinear Model of Sulphation Phenomena in Calcium Carbonate Stones*, IAC report 9, Istituto per le Applicazioni del Calcolo “Mauro Picone,” Rome, Italy, 2003. Available online at <http://www.iac.rm.cnr.it/~natalini/postscript/solf4.pdf>.
 - [13] S. M. HASSANZADEHA AND A. LEIJNSEA, *A non-linear theory of high-concentration-gradient dispersion in porous media*, Adv. Water Res., 18 (1995), pp. 203–215.
 - [14] F. H. HAYNIE, *Deterioration of marble*, Durability Build. Mater., 1 (1982/83), pp. 241–254.
 - [15] D. HILHORST, R. VAN DER HOUT, AND L. A. PELETIER, *The fast reaction limit for a reaction-diffusion system*, J. Math. Anal. Appl., 199 (1996), pp. 349–373.
 - [16] D. HILHORST, R. VAN DER HOUT, AND L. A. PELETIER, *Nonlinear diffusion in the presence of fast reaction*, Nonlinear Anal., 41 (2000), pp. 803–823.
 - [17] B. G. D. HOKE AND D. L. TURCOTTE, *Weathering and damage*, J. Geophys. Res., 107 (2002), 2210.
 - [18] N. P. KULSHRESHTHA, A. R. PUNURU, AND K. L. GAURI, *Kinetics of reaction of SO₂ with marble*, J. Mater. Civil Engrg., 1 (1989), pp. 60–72.
 - [19] W. T. LIPPERT, *Atmospheric damage to calcareous stones: Comparison and reconciliation of recent experimental findings*, Atmos. Environ., 23 (1989), pp. 415–429.
 - [20] A. M. MEIRMANANOV, *The Stefan Problem*, de Gruyter, Berlin, 1992.
 - [21] D. A. NIELD AND A. BEJAN, *Convection in Porous Media*, Springer, Berlin, 1992.
 - [22] TH. SKOULIKIDIS AND E. PAPA-KONSTANTINO-U-ZIOTIS, *Mechanism of sulphation by atmospheric SO₂ of the limestones and marbles of the ancient monuments and statues*, I. *Observations in situ (Acropolis) and laboratory measurements*, British Corrosion J., 16 (1981), pp. 63–69.
 - [23] TH. SKOULIKIDIS AND D. CHARALAMBOUS, *Mechanism of sulphation by atmospheric SO₂ of the limestones and marbles of the ancient monuments and statues*, II. *Hypothesis concerning the rate determining step in the process of sulphation, and its experimental confirmation*, British Corrosion J., 16 (1981), pp. 70–76.
 - [24] I. STAKGOLD, *Gas-solid reaction with porosity change*, in Proceedings of the Conference on Nonlinear Differential Equations, Electron. J. Differ. Equ. Conf. 5, Southwest Texas State University, San Marcos, TX, 2000, pp. 247–252.
 - [25] J. SZEKELY, J. W. EVANS, AND H. Y. SOHN, *Gas-Solid Reaction*, Academic Press, New York, 1976.
 - [26] S. TAMBE, K. L. GAURI, S. LI, AND W. G. COBOURN, *Kinetic study of SO₂ reaction with dolomite*, Environ. Sci. Technol., 25 (1991), pp. 2071–2075.
 - [27] R. S. VARGA, *Matrix Iterative Analysis*, Prentice-Hall, Englewood Cliffs, NJ, 1962.